



Fluoride removal by low-cost adsorbents

Fredrik Bernheim

VT 2022

Bachelor thesis: 30 hp

Subject area: Chemistry

School of Science and Technology, Örebro university.

Supervisor: Viktor Sjöberg

Examiner: Stefan Karlsson

Abstract

Fluoride, the most abundant form of fluorine, is an ion released into the environment, mainly via anthropogenic sources and erosion of mineral rocks. Although the element is well known for its health benefits on teeth and bones, it can as well be a harmful pollutant. In some areas on earth, the population can not obtain drinking water that is below the guideline limits of fluoride, which is set to 1.5 mg/L by the world health organization (WHO). Therefore there is a relevance to develop methods that can clean the waters from excess fluoride. The potential problems when it comes to finding these types of methods is that they can be expensive. However, materials generated as residues in industrial processes may be low in cost. In this thesis, silicon reduced AOD-slag, a material generated as a by-product from the production of stainless steel, was examined by its fluoride adsorption behavior and adsorption capacity. The concentrations of fluoride were measured with ion chromatography (IC) and the concentration of metals were analyzed with microwave plasma atomic emission spectroscopy (MP-AES). Additionally pH and conductivity were measured. The functionality of the material surface was analyzed with isotherm modeling, where the Sips isotherm model was tested. Moreover, optimization of the slag was performed by heat treating the material, as well as a sorption kinetics test on both optimized and original slags. The results from the analysis indicated that the material corresponds well to the Sips isotherm. Considering this result it is suggested that at low concentrations, the surface can be characterized as heterogeneous, with different binding energies at different available sites. At higher concentrations the Sips-model explains the surface to be saturated when a monolayer of fluoride is formed. Therefore the binding on the slag surface can be described to have an inner-sphere and covalent character. The metal analysis showed that calcium ions are released from the slag when in aqueous solutions. The presence of calcium in the liquid samples are believed to result in formations of solid calcium fluoride (CaF_2), precipitated on the slag surface. Lastly, the maximum fluoride removal is believed to differ between different types of AOD-slag, where there as well are possibilities to optimize the material.

Keywords: Fluoride, calcium, adsorption, surface precipitation, pH, AOD-slag, ion chromatography, MP-AES, isotherms, Langmuir, Freundlich, Sips.

List of abbreviations

AOD	Argon oxygen decarburization
IC	Ion-chromatography
L/S	Liquid to solid ratio
LOQ	Limit of quantification
MP-AES	Microwave plasma atomic emission spectroscopy
PZC	Point of zero charge

Table of content

ABSTRACT	1
LIST OF ABBREVIATIONS	2
1. INTRODUCTION.....	4
1.1 FLUORIDE	4
1.2 ADSORPTION	5
1.3 ARGON OXYGEN DECARBURIZATION METHOD AND SLAG FORMATION	7
1.4 AIM	8
2. MATERIALS AND METHODS	8
2.1 EXPERIMENTAL DESIGN	8
2.2 PREPARATION OF THE MATERIALS	8
2.3 INSTRUMENT, SETTINGS AND CALIBRATIONS	9
2.4 ADSORPTION AND OPTIMIZATION OF THE SLAG	10
2.5 SORPTION ISOTHERMS	10
2.6 SORPTION KINETICS	11
3. RESULTS AND DISCUSSION	12
3.1 ORIGINAL SLAG	12
3.1.1 <i>Visual aspects of the slag</i>	12
3.1.2 <i>Adsorption test</i>	12
3.1.3 <i>pH/Conductivity</i>	16
3.1.4 <i>Metal ions</i>	17
3.1.5 <i>Isotherm modeling</i>	20
3.1.6 <i>Kinetics</i>	24
3.2 OPTIMIZATION OF THE SLAG	25
3.2.1 <i>Visual aspects of the slag</i>	25
3.2.2 <i>Adsorption test</i>	25
3.2.3 <i>pH/Conductivity</i>	26
3.2.4 <i>Metals</i>	26
3.2.5 <i>Isotherm modeling</i>	26
3.2.6 <i>Kinetics</i>	27
4. CONCLUSIONS	28
ACKNOWLEDGMENTS	28
5. REFERENCES.....	29
APPENDIX.....	31

1. Introduction

1.1 Fluoride

Fluorine is a common element on earth. With its strong oxidizing potential it is the element with the highest electronegativity (Sivasankar et al., 2013) and has consequently a strong tendency to gain an electron. Therefore it is rather found as an anion, fluoride (F^-) than in its elemental form, and can easily form mineral complexes with numerous cations. These complexes exist naturally in the earth's crust (WHO, 2006), and when weathered, the ions get distributed into the environment (IPCS, 2002). Fluoride can additionally be released through anthropogenic sources, for instance as a result of waste from industrial processes in the production of various materials (IPCS, 2002). In the environment fluoride may be found in soil, water and air, while in the human body, fluoride is mainly ingested via food and water. The majority of the ions that are ingested get adsorbed in the gastrointestinal tract, and are from this point distributed to and integrated with the crystal lattice in teeth and bones (IPCS, 2002). This incorporation is reversible and fluoride can further be excreted through the body (IPCS, 2002).

The effects of fluoride on humans can result in both beneficial as well as adverse outcomes. A typical beneficial usage of fluoride is on teeth. Its protection against caries in the right amounts is considered to be a healthy substitute in toothpaste and water. However, the ions can also cause harmful effects (IPCS, 2012). India as an example has a reported problem regarding calcium fluoride minerals. These minerals are the source of fluoride contaminations of food and waters all around the country. In areas where the inhabitants don't have the opportunity to obtain fluoride treated drinking water, an unhealthy intake of fluoride can cause skeletal fluorosis. This disease can have adverse effects on bones and joints, thus reducing the body mobility (Del Bello, 2020). The problem is not exclusively related to India, and is as well affecting people living in African and Chinese regions (IPCS, 2012). Additional possible harmful effects are cancer, increased risk of bone fractures, infertility, brain damage among others (Patel et al., 2018). Fluoride can therefore be considered as a harmful substance and since it is released into the environment it can be defined as a pollutant (Patel et al., 2018). Due to the possible adverse effects of fluoride, the world health organization (WHO) has expressed a limit guideline value in drinking water to 1.5 mg/L (WHO, 2006). However, the concentrations in waters can differ depending on the water's location in relation to anthropogenic or natural sources of emission (IPCS, 2002). For this reason nearby areas to an emission source can, due to the naturally high fluoride concentrations, have difficulties in meeting the guideline limits (WHO, 2006).

Clean drinking water is an important question and with pollutants contaminating the waters there is a relevance for remediation treatments. Since fluoride can be considered a harmful pollutant and since there are waters containing fluoride all around the world, the development of convenient remediation methods for these types of pollutants can have an important role in cleaning the waters. The opportunities to find treatment techniques for contaminated waters

are promising where an interesting area is the use of materials that are capable of adsorb the pollutant. Considering fluoride, there are developed techniques which have shown to be beneficial of removing fluoride in water, which include sorbents such as activated carbon and activated alumina (Patel et al., 2018). Activated carbon has proved to be a highly convenient adsorbent of fluoride. However, it is as well related to high costs (Foo and Hameed, 2009) which shows that there is a relevance to find materials of low costs that as well are favorable fluoride sorbents.

1.2 Adsorption

The adsorption theory is a general description of the process where components in a gas or a liquid get attracted and bind to a solid surface (Foo and Hameed, 2009). In terms of a solid-liquid system, the adsorbate is the definition of a liquid compound that binds to the solid surface, where the surface is defined as the adsorbent (Dabrowski, 2001).

Due to these attractions, the components can bind to the solid surface through either chemical or physical interactions (Foo and Hameed, 2009). These types of interactions are classified based on the bond strengths between the adsorbate and adsorbent. Chemical adsorption, or chemisorption, is based on chemical interactions. This results in covalent bonds and an irreversible monolayer of the adsorbed molecules. In physical adsorption, or physisorption, electrostatic interactions between the adsorbate and adsorbent takes place (Al-Ghouti and Da'ana, 2020). The electrostatic interactions are weaker than the chemical and include bonding by forces such as Van der Waals and dipole-dipole (Al-Ghouti and Da'ana, 2020)(Wang and Guo, 2020). Moreover, in comparison to chemisorption, physisorption can form a multilayer of the adsorbate on the surface (Al-Ghouti and Da'ana, 2020).

In order to more thoroughly describe a general surface, the surface complexation model can be used. In general, surface complexation can be explained as outer- and inner-sphere adsorption. Outer-sphere adsorption, just as physisorption, is defined as electrostatic forces that causes a charged surface to attract an adsorbate with the opposite charge. The adsorbate is not directly bounded to the surface, where there rather is at least one layer of water molecules between the adsorbate and the surface. The reactions rates in outer-sphere adsorption are fast where it takes minutes or even seconds for the reactions to occur. Inner-sphere adsorption can in comparison be explained similar to chemisorption, as stronger chemical interactions where there are covalent or strong ionic bonds formed. The initial reactions in inner-sphere adsorption are quite fast, however compared to outer-sphere reactions the rate decreases over time, which makes the adsorption process last longer (Strawn et al., 2015). The initial process during adsorption include an external mass transfer where the adsorbate reaches the external surface of the material. This is followed by an intra-particle diffusion where the adsorbate penetrates the porous layer of the material. Lastly the adsorption takes place, where the adsorbate binds to the active site of the material. The pore structure, including pore size, porosity and pore morphology, have shown be a limiting factor in the rate of the adsorption process. Therefore, even though both inner- and outer-sphere processes have differences in their sorption kinetics, the rate is primarily determined by the pore structure of the material. (Wu et. al., 2022).

Since the adsorption can differ depending on what type of material that is being used, isotherm models can be used to provide information about the adsorption behavior (Al-Ghouti and Da'ana, 2020). Isotherms can be used to illustrate the equilibrium relationship in a system at a constant temperature, between the concentration of a compound in a liquid phase and the amount adsorbed to a surface. A system is considered to be in chemical equilibrium when the adsorbate has been in contact with the adsorbent for a sufficient amount of time and there is no further change of concentration in neither the liquid nor on the solid surface (Al-Ghouti and Da'ana, 2020). The isotherm models can then provide important data that explain the adsorption capacity and the adsorption mechanisms of the adsorbent, including bonding energies and bond types (chemical or physical) at the binding sites of the surface. Isotherms are hence essential models when it comes to evaluate and express how a surface material adsorbs certain components. An adsorption isotherm can be illustrated as a curve based on the concentrations of adsorbate in the liquid and on the solid phase, which characterizes the relationship between these concentrations. (Foo and Hameed, 2009)(Wang and Guo, 2020). In this study there will be three different isotherms discussed, Langmuir- and Freundlich isotherms as two-parameter models and Sips isotherm as a three-parameter model.

Considering the sorption of fluoride, it has previously been reported that compounds with high content of calcium can be effective adsorbents. One example is a study made on eggshells which has a high concentration of calcium carbonate (CaCO_3), representing approximately 94% of the total content. Analysis of the adsorption capacity of fluoride indicated that thermal treatment of the eggshells promoted the adsorption of fluoride. After thermal treatment at temperatures between 800-900°C, adsorption was most effective which was believed to be a result of the formation of calcium hydroxide (Ca(OH)_2) and calcium oxide (CaO) (Lee et al., 2021). This indicate that calcium rich materials are of interest when it comes to adsorption of fluoride, and that there is a possibility to optimize these kind of materials. Another element of interest in terms of fluoride removal is aluminum. Previous studies have shown that materials containing aluminum oxide (Al_2O_3) promote the formation of the adsorption complex aluminum fluoride (AlF_3). The formation of this complex can thus reduce the concentration of free fluoride in liquid solutions (Dolganov et al., 2021).

The adsorption capacity can as well be affected by the solution and its properties such as ionic strength, temperature and pH (Al-Ghouti and Da'ana, 2020). Regarding the sorption characteristics of an adsorbent surface, the pH of the solution is of interest and can be explained by point of zero charge (PZC). PZC is defined as the point where the surface charge of a material is equally negative as positive. At conditions where the pH is below pH_{PZC} the surface is protonated, resulting in a more positively charged surface. At pH above pH_{PZC} the surface is more negatively charge as a result of deprotonation (Strawn et al., 2015). Previous studies have shown that the adsorption capacity of fluoride on calcium rich materials have a significant decrease when the pH increases. The reason for this is that the net charge of the surface is affected by the pH and an increase of pH leads to a more negatively charged surface of the adsorbent (Lee et al., 2021)(Muhammad et al., 2019). These results

could be an indication that the pH of the samples are above the pH_{PZC} , resulting in a negatively charge surface and a repulsion of negatively charged fluoride.

Lastly, studies have shown that clays made of hydrocalumite, a mineral containing calcium, can release calcium ions (Ca^+) when in fluoride solutions. The dissolution of Ca^+ can then result in a precipitation of calciumfluoride CaF_2 (Habuda-Stanić, 2014). The precipitation of CaF_2 could as well be affected by the pH, where a high concentration of OH^- in a solution with calcium and fluoride could result in formations of $\text{Ca}(\text{OH})_2$ over CaF_2 . Due to the presented information it is suggested that there are multiple mechanisms affecting fluoride removal.

1.3 Argon Oxygen Decarburization method and slag formation

One type of material that might be used for adsorption is industrial residues, which are considered to be environmentally friendly, easy to use and very cost effective (Patel et al., 2018). During the manufacturing of iron and steel, various types of slags are formed as by-products. By removing unwanted compounds, the processes resulting in the formation of slags are fundamental in order to give the product its desired properties. Depending on what type of process the producer is using, different kinds of slags can be generated. These by-products are of interest since there is a potential for them to be used as a water cleaning materials. Plenty of countries around the world are already using slag products for this purpose, mainly for the adsorption of phosphorus in aqueous solutions (Jernkontoret, 2018).

The Argon Oxygen Decarburization (AOD) process is one of the methods that can be used for the production of stainless steel, resulting in the formation of AOD-slag. The process can be separated into three main steps that takes place in an AOD-converter;

1. Decarbonization, where the carbon content is reduced by adding oxygen and argon through the melted steel. This procedure will generate metal oxides in the slag.
2. Reducing elements such as silicon and aluminum are added in order to reduce the oxidized metals. Calcium is as well added due to its affinity to sulfur and metals. Slag containing lime together with silicon- and aluminum oxides will be generated.
3. Calcium oxide (CaO) is added in order to reduce the amount of sulfur. This step is necessary since sulfur, even in small amounts, can damage the properties of the steel (Jernkontoret, 2018).

The final by-product is a slag material, and when cooled it creates a material consisting of various minerals (Jernkontoret, 2018). According to Li J. et al. (2016) analysis of air cooled AOD slag and its composition, the AOD-slag contains a large amount of calcium oxide (CaO) as well as lower amounts of other oxides, for instance silicon dioxide (SiO_2) and aluminum oxide (Al_2O_3). Since AOD-slag has been shown to contain both calcium as well as aluminum, the AOD-slag may be of interest when it comes to adsorption of fluoride. By 2019 it was estimated that around 1.8 billion tons of AOD-slag is generated each year, suggesting that large amounts of possible water-cleaning materials might be available (Wang et al., 2019).

1.4 Aim

The aim of this bachelor thesis is to examine the fluoride adsorption characteristics of six AOD-slugs generated from six different AOD-processes. The characteristics of the slugs are aimed to be illustrated by the adsorption capacity and sorption kinetics when in solutions containing deionized water and dissolved sodium fluoride (NaF). Furthermore, isotherm modeling will be used to illustrate the adsorption capacity of fluoride and what type of bonding that occurs on the slug surface. The hypothesis is that AOD-slug can be optimized and used as a fluoride adsorbent.

2. Materials and methods

2.1 Experimental design

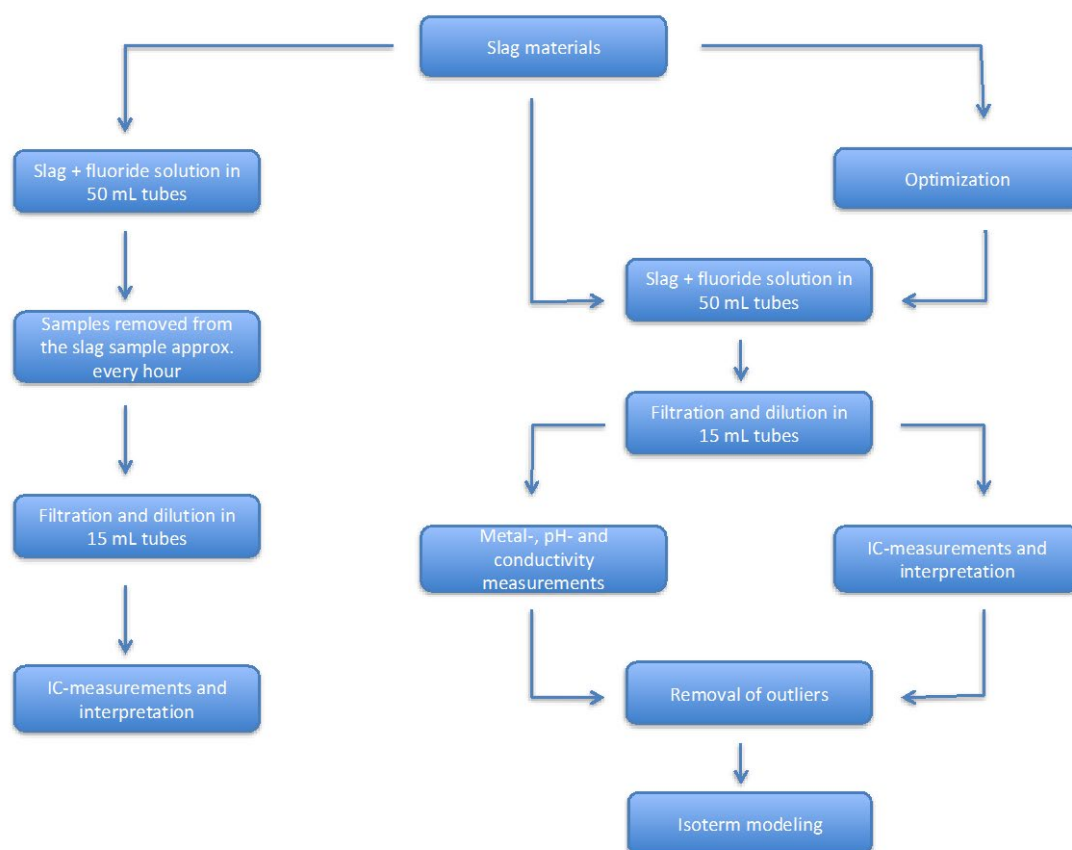


Figure 1. Graphical illustration of experimental design

2.2 Preparation of the materials

The six AOD-slugs to be analyzed were labeled 10738L, 10738V, 10761L, 10761V, 10771L and 10771V, and were obtained from Outokumpu, a manufacturer of stainless steel in Avesta, Sweden. The numbers in the slug names represent a difference of the manufacturing processes of the AOD-slugs, which differs depending on the desired properties of the final

product. The letters L and V represent if the slag during the AOD process had been cooled in air or in water, respectively. Generally the slag materials were delivered in size fractions between 0.9-2.0 mm. Moreover, 10761 are of particular interest since this is the most generated slag type. In order to obtain the concentrations used as the adsorbate aliquots, fluoride standards were prepared by dissolving sodium fluoride (NaF) in 50-mL polypropylene(PP)-tubes (Sarstedt ®) with deionized water.

2.3 Instrument, settings and calibrations

Anions were quantified in filtered solutions (0.20-µm polypropylene syringe filters) with ion chromatography using a Dionex AS12A column with a Dionex AG12A guard. The running buffer of 10.5 mM Na₂CO₃/0.5 mM NaHCO₃ was used at a flow rate of 1.5 mL/min. Conductometric detection was made after suppression, using deionized water and sulfuric acid (H₂SO₄)(50-70 mM), respectively. Dual injections were made, and the concentrations reported as their average. External calibration was performed daily, prior to sample analysis, with five calibration solutions containing fluoride concentrations of 0.1, 0.5, 1, 3 and 10 mg/L. The multistandard calibration solutions were prepared by dilution of stock solutions containing 1 g/L of each anion, with sodium as the counter ion, in de-ionized water (18.2 MΩ). Calibration blanks containing de-ionized water (18.2MΩ) was freshly prepared before each calibration. The IC-Net software (Metrohm) was used for manual inspection of each chromatogram and integration of peak areas.

For pH and conductivity measurements, a Metrohm 914 pH/Conductometer was used to measure all samples used for the adsorption tests. The instrument was operating in drift-dependent mode and equipped with a Metrohm 6.0260.010 pH probe and a Metrohm 6.0917.080 conductivity cell. However, due to issues with the conductivity cell, only a small portion of the samples were able to be measured. Calibration was made daily prior to the measurements.

All samples used in the adsorption tests, which include all original slag types as well as the optimized 61V slag, were analyzed for the content of selected metals. Calcium (Ca) (616.217 and 422.673 nm), aluminum (Al) (394.401 and 396.152 nm), sodium (Na) (88.995 and 589.592 nm), magnesium (Mg) (285.213 and 383.829), iron (Fe) (371.993 and 373.486), manganese (Mn) (403.076 and 403.307) and potassium (K) (766.491 and 769.897) were analyzed. Calcium, aluminum, magnesium, iron and manganese were measured due to their high affinities to fluoride. Sodium and potassium were measured due to their ion strength in water. Prior to the analysis, the samples were acidified with concentrated nitric acid (HNO₃) (1% w/w). The samples were injected three times with an uptake time of 90 seconds, and a rinse time of 90 seconds using nitric acid. The pump speed was set to 10 rpm and stabilization time was set to 15 seconds. Viewing position and nebulizer flow (L/min) were optimized using the function for optimization. Calibration was made prior to the analysis with one blank and 4 standard solutions containing 0.01, 0.1, 1 and 10 ppm of the elements to be analyzed.

2.4 Adsorption and optimization of the slag

The adsorption of fluoride to the slag was tested using a liquid to solid ratio (L/S) of 100. For each test was a 50 mL tube loaded with slag (0.2 g) and then was deionized water and fluoride standard added to reach the desired fluoride concentration and a total volume of 20 mL. The prepared samples were left at room temperature to reach chemical equilibrium. After approximately 24 h was the aqueous phase sampled and the solutions were filtered through 0.2 µm filters (VWR ®) into 15 mL PP-tubes (Sarstedt ®) using 10 mL sized syringes (B.Braun ®). The obtained solution was analysed using IC after appropriate dilution using deionized water. To determine the initial concentrations of fluoride, samples without the addition of slag but with the same concentrations were prepared and analyzed. For the original slag, a test with slag and deionized water was performed in order to determine whether the slag releases fluoride. The amounts of fluoride adsorbed to the slags (mg/g) were calculated with the following equation:

$$q_e = \frac{C_i - C_e}{m} * V$$

Where q_e is the concentration of fluoride adsorbed to the slag surface (mg/g), C_i is the fluoride concentration in the samples without addition of slag (mg/L), C_e is the concentration of fluoride in the solution after equilibrium between the solid and aqueous phase (mg/L), m represents the mass of AOD-slag added to the solution (g) and V is the total volume of the aqueous solution (L). The q_e and C_e results were used as parameters in the isotherm modeling. It would as well be possible to use mMol/g as a unit for sorption. But since there is only one ion measured, the unit mg/g was applied.

Paired t-tests were performed on the q_e -results from the adsorption tests, with a significance level of 0.05. The t-tests were made in order to compare the air cooled against the water cooled slags. Additionally the differences were illustrated by plotting the q_e -values of the compared slag samples against each other to demonstrate any potential visual differences. The null hypothesis of the paired t-test is that there are no differences between the air cooled and water cooled slags.

As a second part of the adsorption investigation, the slags were optimized by heating. The optimization occurred at a temperature of 900°C for approximately 6 hours in a Muffle furnace. The optimized slags were further prepared and analyzed in the same way as the unoptimized slags.

2.5 Sorption isotherms

The three parameter Sips isotherm was tested on all slag types. Since it is a combination of both Langmuir and Freundlich, these two models need to be discussed as well.

The Langmuir isotherm model was developed for surfaces that adsorbs single molecule thick monolayers of adsorbate, meaning that there are only fixed number of sites on the

surface where the adsorbate can bind to. The model assumes a homogeneous surface, meaning that all binding sites of the adsorbent have the same affinities for the adsorbate (Foo and Hameed, 2009). The Langmuir model assumes that there are basically no interactions between adsorbed molecules (Wan and Guo, 2020), as well as no transmigration of the adsorbate, meaning that the binding sites have fixed positions on the surface (Al-Ghouti and Da'ana, 2020). The linear Langmuir isotherm can be expressed with the equation:

$$q_e = \frac{Q_o b C_e}{1 + b C_e}$$

Where q_e is the concentration of fluoride on the surface at equilibrium (mg/g), Q_o is the theoretical maximum capacity of adsorption (mg/g), b is the Langmuir isotherm constant (dm^3/mg) and C_e is the remaining concentration of adsorbate in the solution while at chemical equilibrium (mg/L) (Foo and Hameed, 2009).

Freundlich isotherm can, in comparison to the Langmuir model, be used to describe multilayer adsorption. In this isotherm the surface is assumed to be heterogeneous, meaning that there are differences in bond strengths at different bonding sites. During adsorption this will result in a bonding of adsorbate to stronger binding sites at first, with an exponential decrease in binding energies. The information provided by the model can indicate the adsorption intensity, meaning how heterogeneous a surface is. The model can be described with the equation:

$$q_e = K_f C_e^{1/n}$$

Where K_f is the Freundlich isotherm constant ($\text{mg/g})(\text{dm}^3/\text{g})^n$ and n represents the adsorption intensity as a number between 0 and 1, where the closer the value is to 0, the more heterogeneous the surface is (Foo and Hameed, 2009).

The Sips isotherm is a three parameter model which can be described as a combination between the Langmuir and Freundlich isotherms. Just like Freundlich the model assumes a heterogeneous surface with different bond strengths at different sites, which can explain the adsorption behavior at lower concentrations of adsorbate. Furthermore the Sips model, similarly to Langmuir model, assumes a monolayer adsorption. This means that the sorption capacity has an upper limit, which can explain the adsorption characteristics at higher concentrations of adsorbate. The Sips model can be described with the following equation:

$$q_e = \frac{K_s C_e^{\beta_s}}{1 + a_s C_e^{\beta_s}}$$

Where $K_s(\text{L/g})$ and $a_s (\text{L/mg})$ are the Sips isotherm constants and β_s is the Sips isotherm exponent (Foo and Hameed, 2009).

2.6 Sorption kinetics

The time needed for the system to reach chemical equilibrium between fluoride in the solution and fluoride bonded to the slag surface, was measured with a sorption kinetics test. This test was performed on the original as well as the optimized 61 V slag. For each slag, two

50 mL tubes were prepared, one containing 0.2 slag and the other containing a 20 mL solution with a fluoride concentration of 1000 mg/L. Before the fluoride solution was added to the slag, a sample of 100 μ L was transferred into a 15 mL tube and diluted to 10 mL with deionized water. The fluoride sample was then added to the slag sample tube. The sample tube was laid down in room temperature, and at approximately each hour, a sample of 100 μ L mL was transferred from the sample solution into a 15 mL tube and diluted to 10 mL with deionized water. The total volume removed was not more than 10% of the initial volume of the sample. All samples removed and diluted were measured for their fluoride concentrations. The q_e -values were calculated and plotted versus time, in order to illustrate the amount of adsorbed fluoride to the slag in relation to time.

3. Results and discussion

3.1 Original slag

3.1.1 Visual aspects of the slag

By the visual appearance of the slags, there are clearly differences in both sizes and color. First of all there is a difference between the slags cooled in air and the slags cooled in water. In the air cooled slag, the material has a darker color while the water cooled slag has a brighter, light gray tone. Additionally, the appearance of the grains within the same slag types have various characteristics as well. A comparison between individual grains showed differences in both color and in size. The sizes are mainly between 0.9 and 2 mm, but there are as well even smaller grains caused by the grains breaking during sifting and subsequent storing. These characteristics indicate that there are different mineral phases in the slag, formed during the cooling step of the AOD-process. Due to the different mineral phases the slag can break into grains of various sizes and colors. What these differences further are indicating is that there as well could be variations in the sorption capacities depending on the type of mineral phase. This in term indicate that there may be adsorption differences between different types of slag, but also between individual slag grains of the same slag type.

3.1.2 Adsorption test

Initially, all original slags were added to solutions containing deionized water, with no fluoride added. The fluoride analysis of these samples showed that even though no fluoride was added to the samples, fluoride could be found in the liquid phase, shown in table 1. What these result indicate is first of all that the slag contain fluoride, but also that fluoride can be released from the slag surface when in an aqueous solution.

Table 1. Released fluoride from original slags in deionized water.

Slag type	Slag weight (g)	Time of test (h)	Concentration of fluoride after test (mg/L)	Amount of fluoride released (mg/g)
-----------	-----------------	------------------	---	------------------------------------

38 L	0.2024	6.00	1.29	0.127
38 V	0.1963	6.00	0.232	0.0236
61L	0.1961	6.00	0.450	0.0459
61 V	0.1975	6.00	0.444	0.0450
71 L	0.2011	6.00	1.31	0.130
71 V	0.2048	6.00	0.688	0.0672
38 L	0.2056	66.5	4.84	0.471
38 V	0.2089	66.5	0.497	0.0476
61 L	0.1978	66.5	1.68	0.170
61 V	0.2052	66.5	2.99	0.291
71 L	0.2022	66.5	6.03	0.596
71 V	0.2044	66.5	1.30	0.127

At C_e -values (fluoride concentrations in the liquid after equilibrium) of 100 mg/L, positive q_e -values (concentration of fluoride adsorbed to the slag) could be obtained (values are provided in table 11-16 of the appendix). As the C_e -values further increases there is a relatively consistent relationship to increasing q_e -values, seen in figure 2-7. However at C_e -values above somewhere around 1000 mg/L, there is a inconsistency of the results, where the q_e -values show large differences between individual samples. Additionally, at fluoride concentrations above 1000 mg/L, there is an indication that the slags have reached their maximum adsorption capacity. The q_e -values when the C_e -values are above 1000 mg/L are mainly found in interval between 5-15 mg/g.

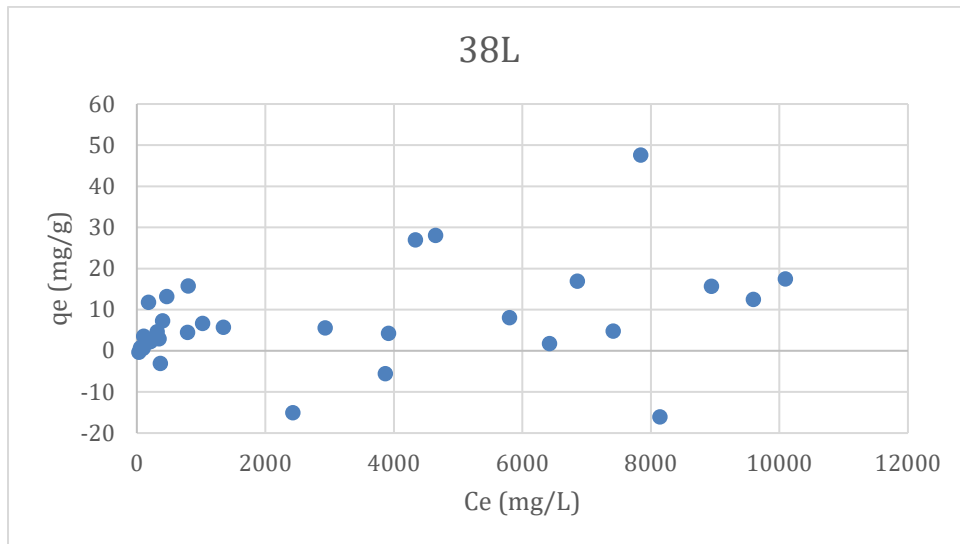


Figure 2. Adsorption of fluoride to the 38L-slag (mg/g) versus concentration of fluoride in the liquid phase.

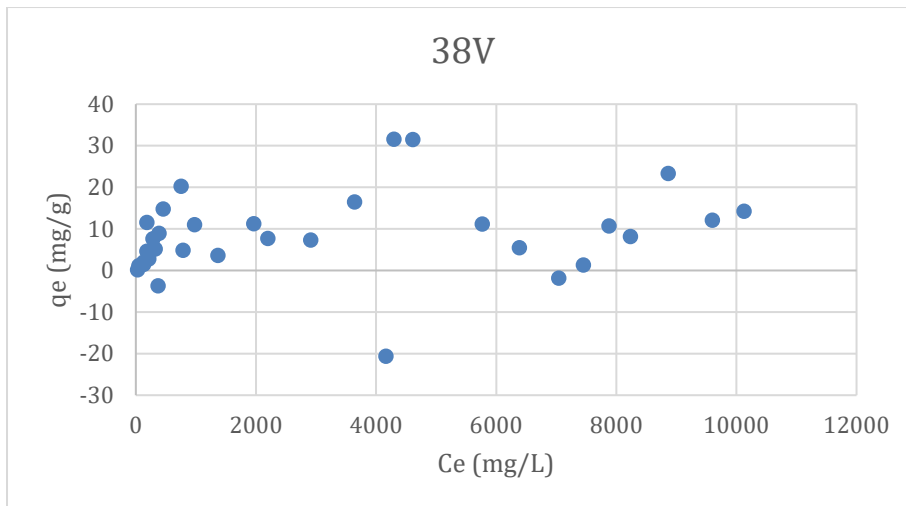


Figure 3. Adsorption of fluoride to the 38V-slag (mg/g) versus concentration of fluoride in the liquid phase.

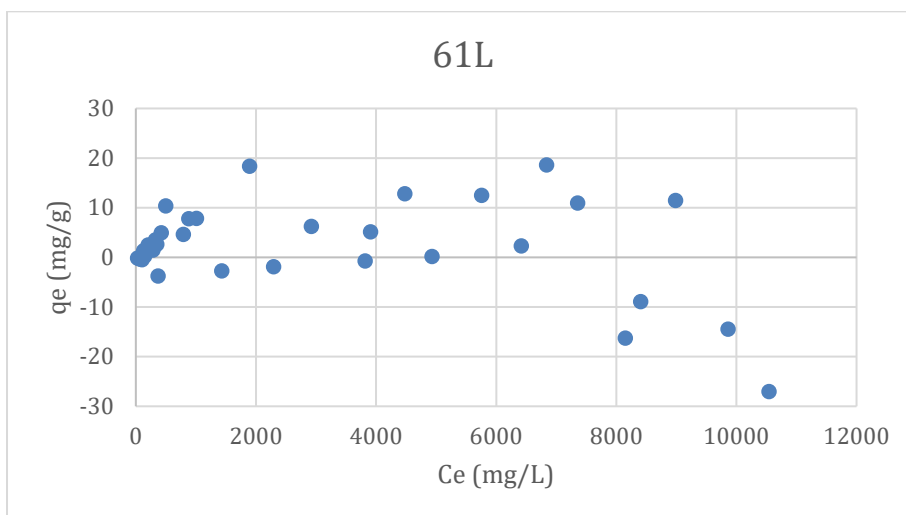


Figure 4. Adsorption of fluoride to the 61L-slag (mg/g) versus concentration of fluoride in the liquid phase.

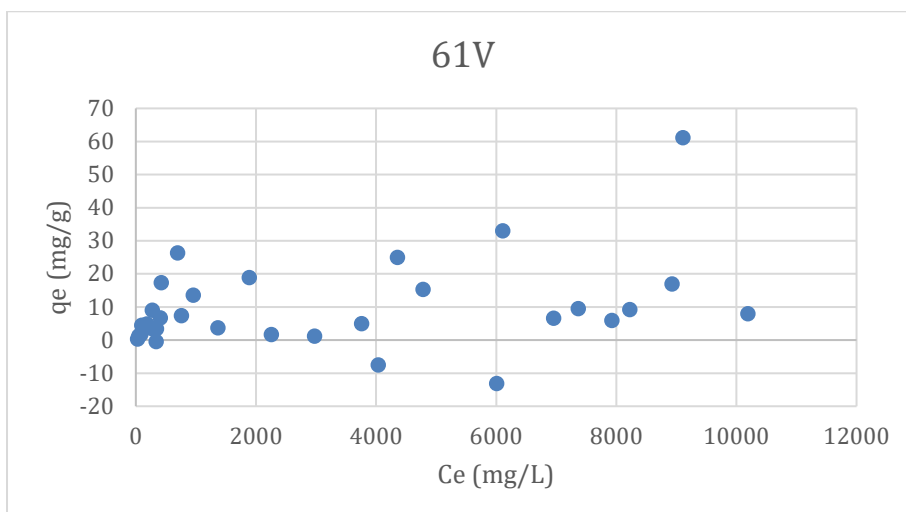


Figure 5. Adsorption of fluoride to the 61V-slag (mg/g) versus concentration of fluoride in the liquid phase.

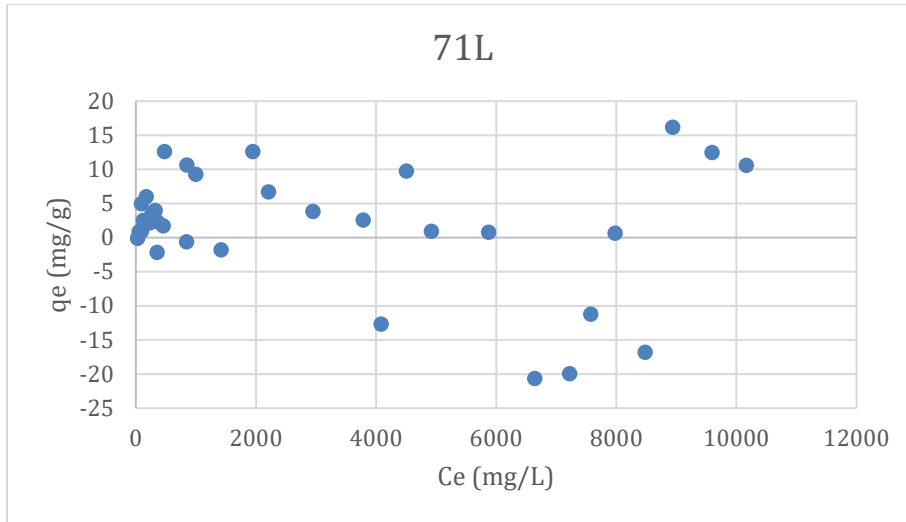


Figure 6. Adsorption of fluoride to the 71L-slag (mg/g) versus concentration of fluoride in the liquid phase.

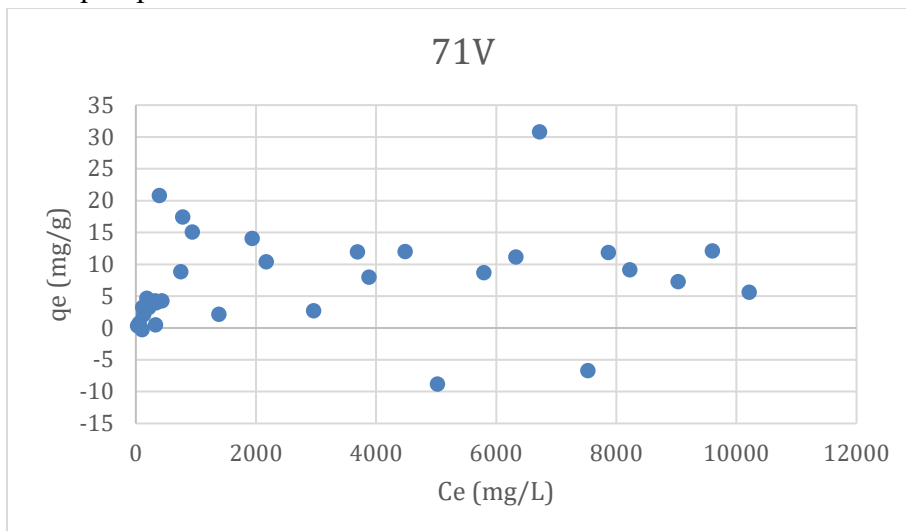


Figure 7. Adsorption of fluoride to the 71V-slag (mg/g) versus concentration of fluoride in the liquid phase.

Due to the large differences between the data points at C_e -values above 1000 mg/L, comparison between the slags was made up to these concentrations. Since the 61 slag type is the most generated slag type, the main focus on the comparison was made on 61L and 61V. A comparison between 61L and 61V can be seen in figure 8, where the slag types are plotted against each other to demonstrate the difference between them. The data points represent the concentration of adsorbed fluoride (q_e) at chemical equilibrium at different initial fluoride concentrations of fluoride (C_i). The samples follow a similar pattern, where 61V have higher q_e -values throughout the whole comparison. A paired t-test was as well made to prove the difference between the slags, where a p-value of 0.0025 was obtained. This rejects the null hypothesis with a significance level of 0.05, meaning that there is a significant difference

between 61L and 61V with a 95% confidence interval. This conclude that there are differences of the slag material depending if the slag has been cooled in air or in water, where the water cooled slag has the higher sorption capacity.

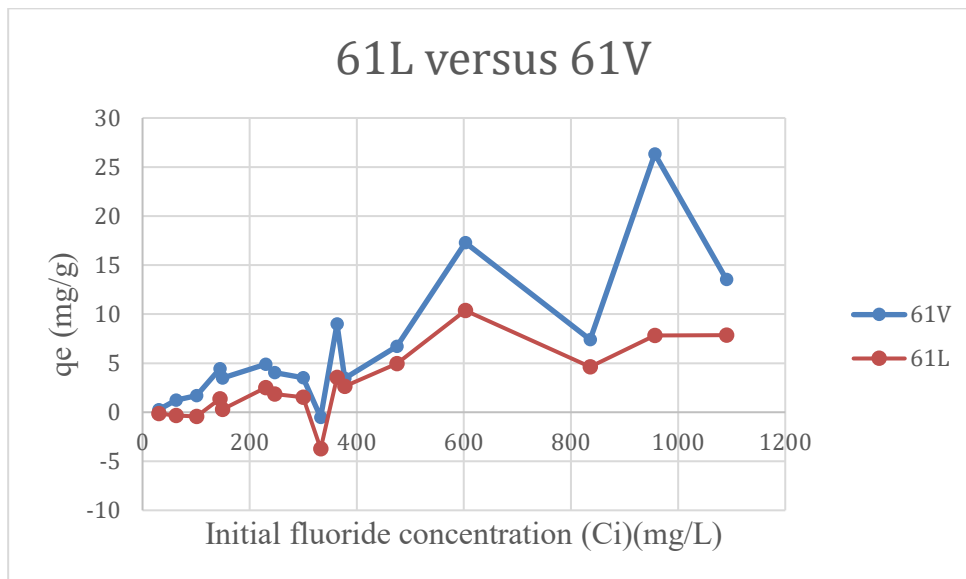


Figure 8. Comparison of sorption between 61L and 61V.

3.1.3 pH/Conductivity

In all samples, the pH of the fluoride solution increased when the slag was added, 61V shown as an example in figure 9. By comparing the slag cooled with air versus with water, there are differences between the two types. When plotted against each other in figure 10, where the data points represent the pH at different initial concentrations, the water cooled slags tend to alter the pH of the solution more than the air cooled.

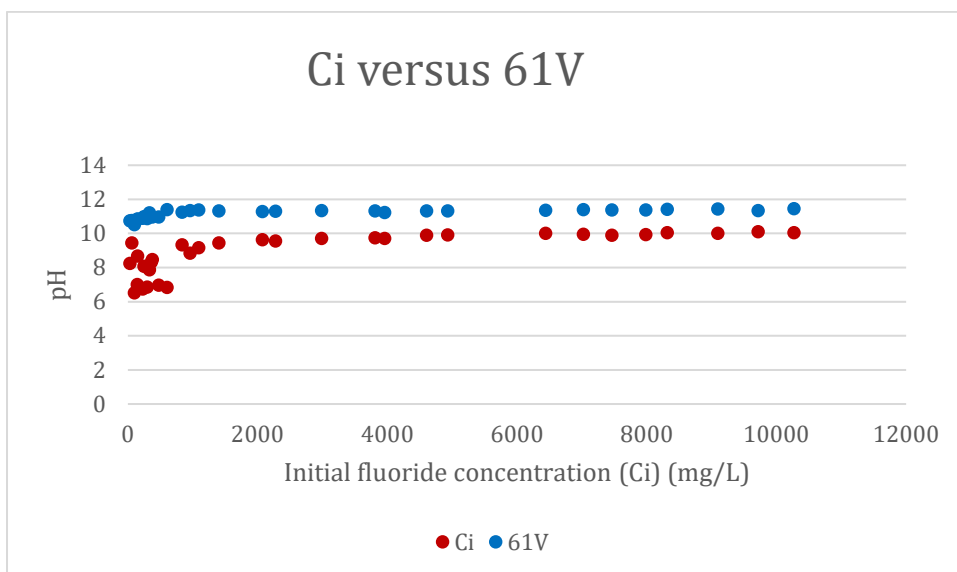


Figure 9. Solution pH comparison of with, versus without added 61V-slag.

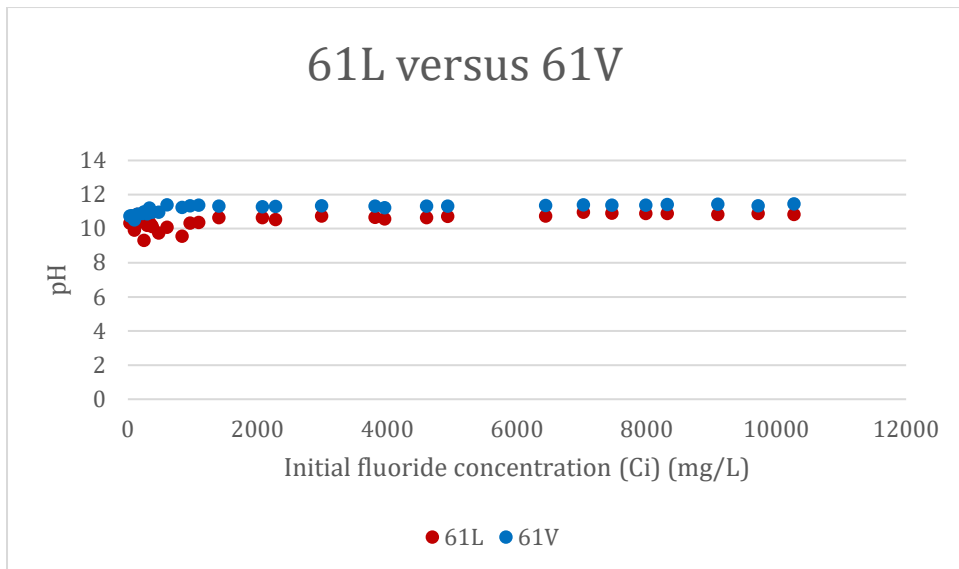


Figure 10. Solution pH comparison of 61L- versus 61V-slag.

As demonstrated in the adsorption test, water cooled slags also have a higher sorption capacity than the air cooled. One likely difference between the surface composition of the two slag types may be connected to what occurs on the slag surfaces when they are cooled during the AOD-process. As previously discussed, air cooled slag contain a high abundance of CaO. However, when the compound CaO is in contact with water, there is a reaction occurring that promotes the formation of $\text{Ca}(\text{OH})_2$. This indicate that the water cooled slag may contain a higher abundance of $\text{Ca}(\text{OH})_2$ than the slag cooled in air. Hence it is possible that a higher abundance of $\text{Ca}(\text{OH})_2$ may be a reason for both an increase in pH as well as a higher sorption capacity. Therefore there would be of interest to further analyze the composition of the water cooled slag surface and how it differs from the air cooled. Moreover, as previously explained, the sorption capacity of fluoride on calcium rich material are influenced by the pH, where lower pH values promote a higher sorption capacity. Considering point of zero charge, it is possible that pH in the samples are above pH_{PZC} , meaning that the solution is not optimal for adsorption. For this reasons it would be of interest to further analyze the pH_{PZC} of the slag, if it differs between air cooled and water cooled and it is possible to obtain a lower pH of the samples in order to increase the adsorption.

The conductivity measurements provided no relevant information regarding the analysis of the slag material. The results from both the pH and conductivity measurements can be found in table 25-30 of the appendix.

3.1.4 Metal ions

The results from the metal analysis of sample liquids showed a large variety of metal concentrations between the samples. In all slag types, there is a negative correlation between detected calcium and the concentration of fluoride, meaning when the concentration of fluoride increases, the amount of calcium decreases (illustrated in figure 17-22). These results suggest two ideas; first is that calcium is dissociated from the slag surface when in contact

with water. Second is that the fluoride removal is influenced by calcium ions in the solution, resulting in a surface precipitation of calcium fluoride (CaF_2 or particle-Ca-F). As illustrated in table 11-16, at C_e -values around 3000 mg/L and higher the amounts of measured calcium are below the limit of quantification (LOQ) of 0.025 ppm. This indicates that around these concentrations of fluoride, there are no more calcium ions present in the solution to further precipitate as CaF_2 . Therefore the calcium is removed as a part of the solid phase and may be the reason for the decreasing amount of calcium at higher fluoride concentrations. This implies that the fluoride removal is not solely explained by an adsorption mechanism, but also as a precipitation set by calcium ions released from the slag. However, as presented in the introduction, since there are more OH^- ions present in the solution at higher pH, there could as well be a formation of $\text{Ca}(\text{OH})_2$. This suggests that there as well could be a precipitation of $\text{Ca}(\text{OH})_2$ in the system and not only CaF_2 .

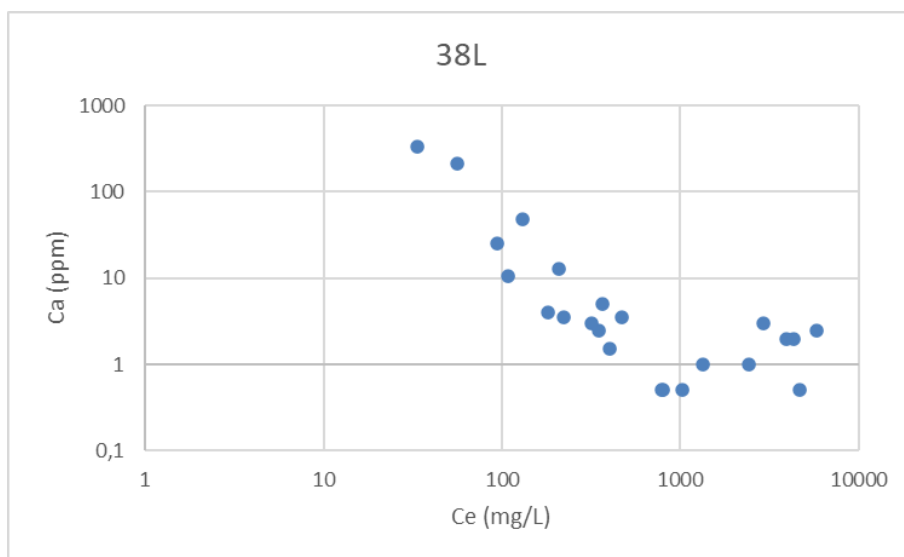


Figure 11. Relationship between fluoride and calcium concentration of 38L-samples.

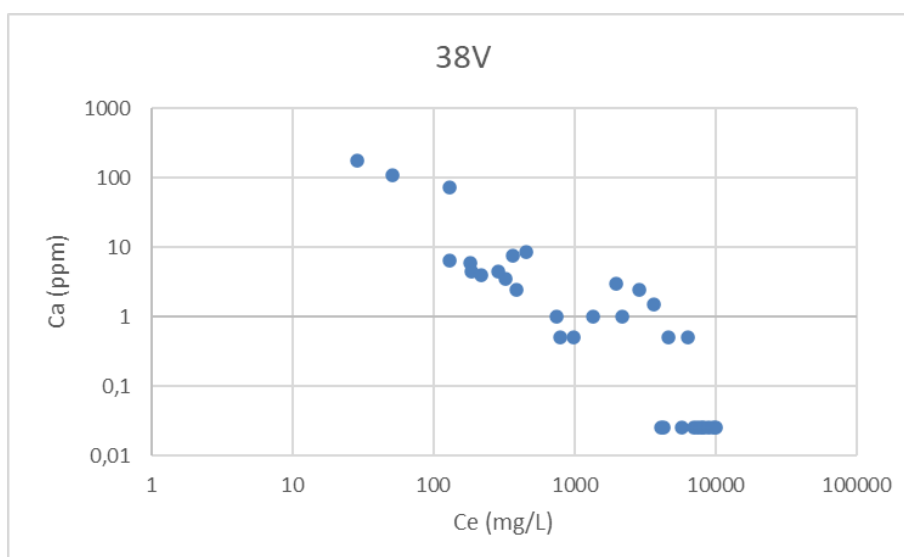


Figure 12. Relationship between fluoride and calcium concentration of 38V-samples.

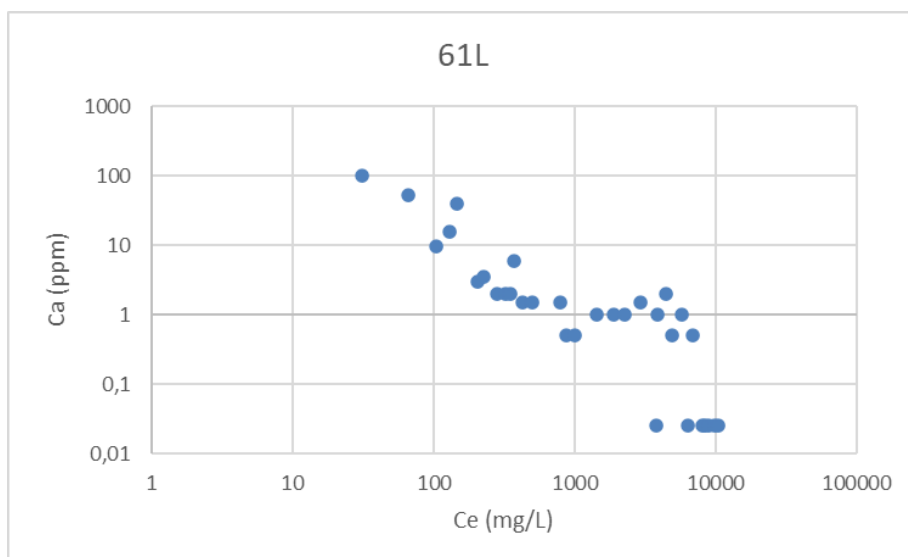


Figure 13. Relationship between fluoride and calcium concentration of 61L-samples.

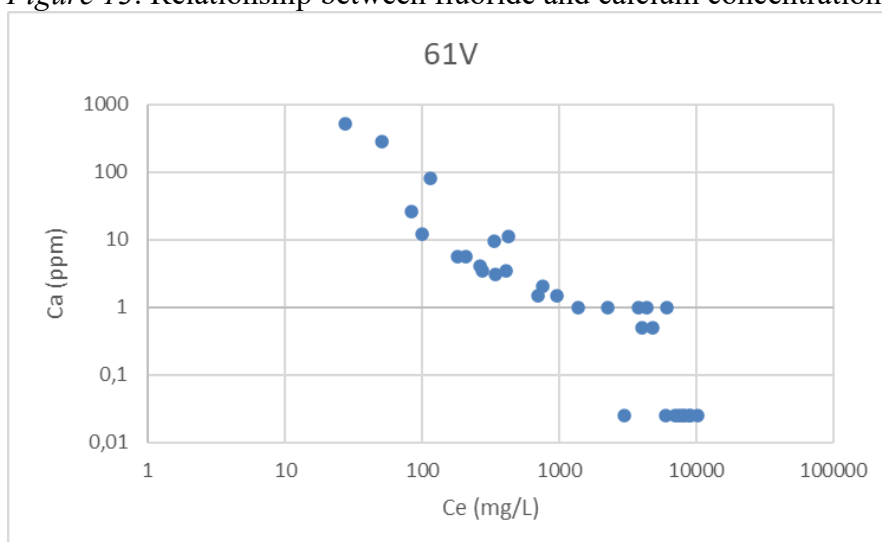


Figure 14. Relationship between fluoride and calcium concentration of 61V-samples.

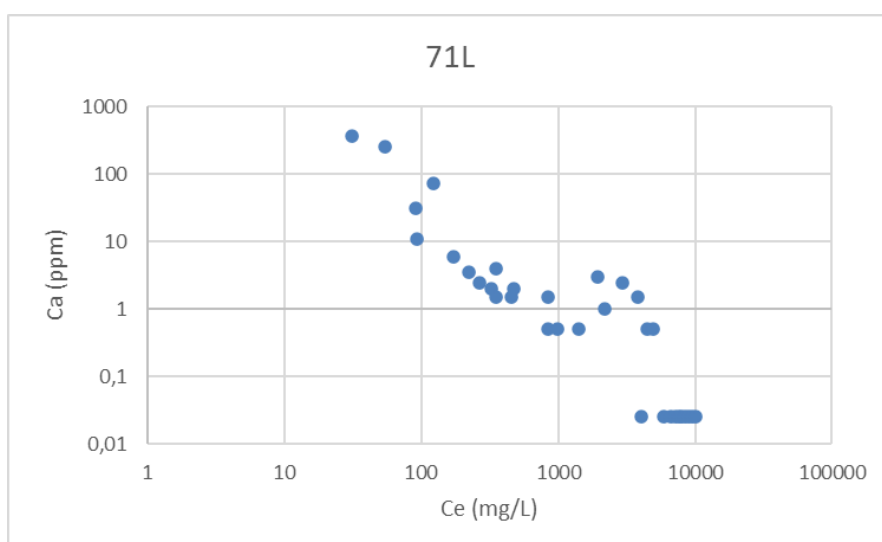


Figure 15. Relationship between fluoride and calcium concentration of 71L-samples.

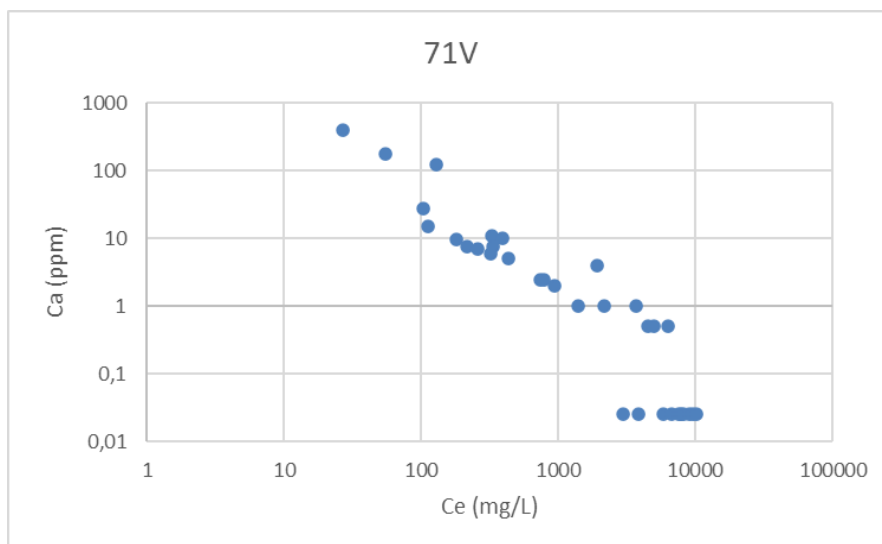


Figure 16. Relationship between fluoride and calcium concentration of 71 V-samples.

The aluminum, sodium and potassium concentrations could not be used in order to provide further information of the slag materials. The results of all metals found can be found in table 18-23 in the appendix. Magnesium, iron and manganese were not detected and is therefore not included in the report.

3.1.5 Isotherm modeling

In order to find relationships between the data points regarding the isotherm modeling, outliers were removed. The outliers were detected in pH, time of the slag in contact with fluoride solution, q_e -values, C_e -values and calcium levels. If the samples were in contact with the fluoride solution longer than 20 hours, and if the pH in the samples were below ten, they were considered as outliers and removed. These data points deviated from the rest and the majority of the samples. Information regarding contact time can be found in table 4-9 of the appendix.

The sorption isotherm models are based on assumptions that adsorption processes are occurring, which is defined by positive q_e -values. If there is no adsorption occurring, i.e. the q_e -values are equal or below 0, they can not be used for the isotherm modeling. Therefore, data points with negative q_e -values were removed. Additionally, in all slag types the vast majority of the q_e -values were in the interval between 0-15 mg/L. Hence there is a probability that a q_e -values above 15 mg/L is most likely due to a irregularity. For this reason, q_e -values above 15 mg/L were considered as outliers and removed. Since the adsorption of the slags most likely reaches their maximum capacity below concentrations of 2500 mg/L, no C_e -values above 2500 mg/L were included in the isotherm analysis.

All data points where the calcium concentration were below the LOQ of 0.025 ppm were removed. As explained, when there are calcium ions in the samples, fluoride is removed by precipitation as CaF_2 . However, as the fluoride binds to calcium, the concentration of calcium decreases. When there are no more calcium in the liquid samples there is an indication that

there are no more mechanism in the system that can cause further removal of fluoride. The most relevant information regarding the sorption is rather how the adsorption changes with the concentration of fluoride. For this reason, samples with no quantified calcium were considered as outliers and hence removed.

The isotherm modeling was performed considering two different assumptions of the slag behavior. As previously discussed there are visual differences between individual slag grains within the same slag type. Therefore the isotherm modeling was in one case performed assuming that there are differences between the individual slag grains due to differences in the mineral phases. This means that differences in color and sizes between slag grains could also have differences in adsorption capacity. Due to the small sample sizes with few slag grains in each sample, a difference in sorption capacity of one or a few grains could potentially have an effect on the fluoride removal of the system. Therefore there may be multiple curves found in the isotherm plots, where each curve represents anomalies in the slag grains. On the other hand it can as well be assumed that the size and color differences between the slag grains are irrelevant and that the sorption capacity does not differ between them.

Figure 17 illustrates the results where the Sips isotherm is adjusted to one curve, assuming that there are no differences between the slag grains. As seen in table 2 the R^2 -values are generally low, which indicate that there are too much differences between the data points to find a correlation that fits the model.

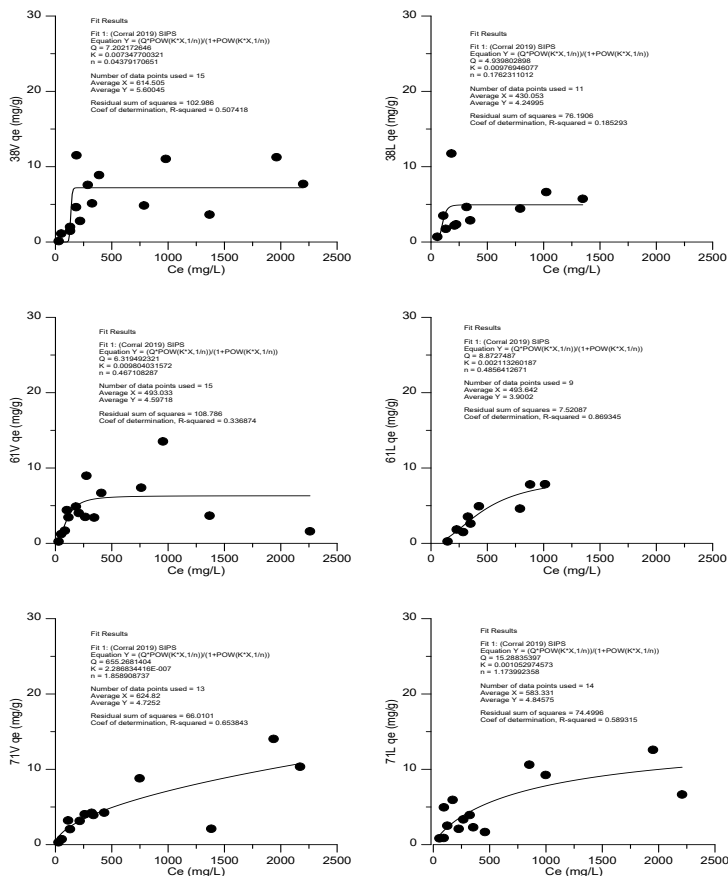


Figure 17. Sips isotherms when assuming no differences in sorption capacity between slag grains.

Table 2. Surface information from the Sips isotherm when assuming no differences in sorption capacity between slag grains.

Slag type	Q (mg/L)	K (L/g)	n	Residual sum of squares	R-squared (R ²)
38L	4.94	0.00977	0.176	76.2	0.185
38V	7.20	0.00735	0.0438	103	0.507
61L	8.87	0.00211	0.486	7.52	0.869
61V	6.32	0.00980	0.467	109	0.339
71L	15.3	0.00105	1.17	74.5	0.589
71V	655	2.29*10 ⁻⁷	1.86	66.0	0.654

A more representative modeling of the Sips was made assuming that multiple curves can be found, where there are clearly higher R²-values obtained, shown in figure x and table x. This can be explained by what has previously been discussed. The reason why the curves differ from each other could be due to differences in mineral structures between individual slag grains, therefore differences in their sorption capacities. The R² also imposes that the slag surface, at concentrations below the maximum sorption capacity, similars the Freundlich model with a heterogeneous surface and a heterogeneous adsorption. The heterogeneous surface influence the shape of the adsorption curve. At lower concentrations the fluoride initially interacts with stronger binding sites with high affinities to fluoride, resulting in a steep slope of the curve. As the stronger binding sites gets occupied, the fluoride will not bind to the remaining weaker sites as easily. This is visualized in the graphs by an evening out on the curve, until the system reaches its maximum sorption capacity which is demonstrated when the curve is a horizontal line. Hence at concentrations where the capacity is reached, the adsorption similar the Langmuir model where a monolayer has been formed. In terms of describing what is occurring on the slag surface, the bonding type can be defined as inner-sphere complex with covalent or strong ionic bonds. This could be the reason why the increase of q_e-values in all slags seem to level out at a certain concentrations of fluoride. According to the isotherm modeling, the maximum adsorption capacity varies greatly between the slag types which indicates that more experiments should be made to obtain a more distinct relationship between the parameters.

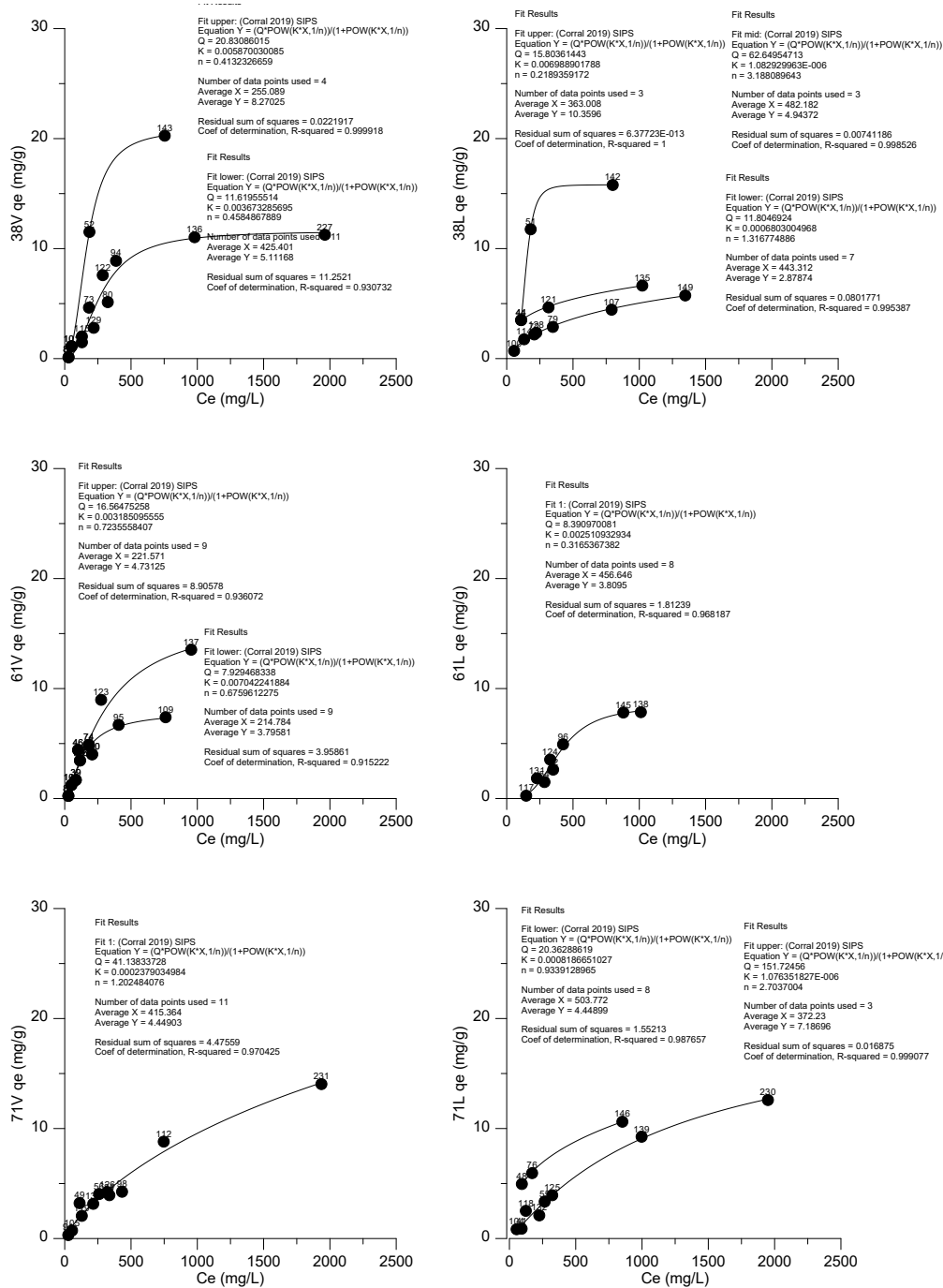


Figure 18. Sips isotherms when assuming a heterogeneous slag.

Table 3. Surface information from the Sips isotherm when assuming a heterogeneous slag.

Slag type	Q (mg/L)	K (L/g)	n	Residual sum of squares	R-squared (R ²)
38L upper	15.8	0.00698	0.219	6.38*10 ⁻¹³	1.00
38L middle	62.7	1.08*10 ⁻⁶	3.19	0.00741	0.999
38L lower	11.8	0.000680	1.32	0.0802	0.995
38V upper	20.8	0.00587	0.413	0.0222	0.999

38V lower	11.6	0.00367	0.458	11.3	0.931
61L	8.39	0.00251	0.317	1.81	0.968
61V upper	16.6	0.00319	0.413	8.91	0.936
61V lower	7.93	0.00367	0.459	3.96	0.915
71L upper	152	1.08×10^{-6}	2.70	0.0169	0.999
71L lower	20.4		0.934	1.55	0.988
		0.000819			
71V	41.1	0.000238	1.20	4.48	0.970

3.1.6 Kinetics

The results from the kinetic-tests of unoptimized 61V-slag showed a chemical equilibrium time of approximately 3-4 hours and an adsorption capacity just below 8 mg/g.

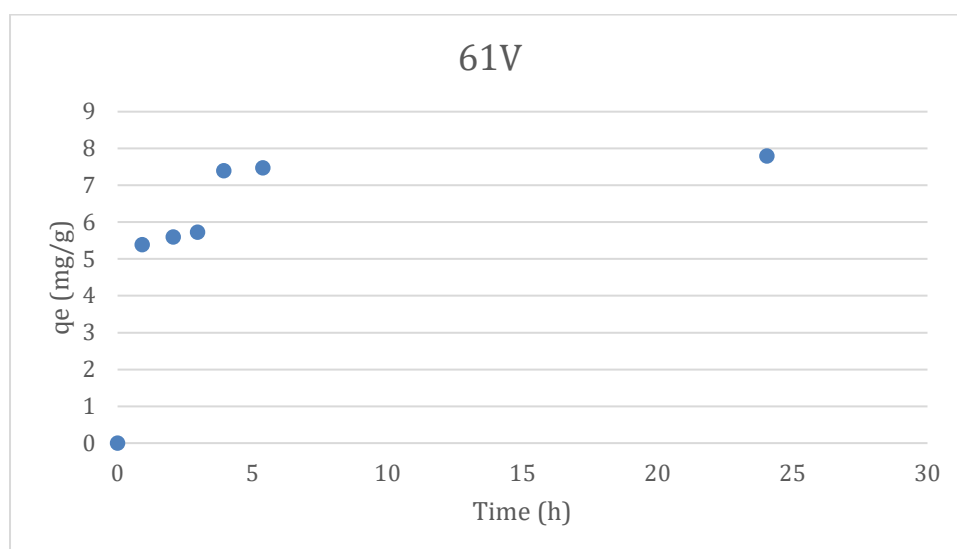


Figure 19. Adsorption of fluoride to unoptimized 61V-slag (mg/g) versus hours of contact between slag and fluoride solution.

The initial rate of the system is rapid, but the longer time fluoride and slag are in contact, the more the rate decreases. Considering outer- and inner-sphere complexes the results are again similar to the inner sphere complex, meaning that there are covalent or strong ionic bonds formed on the surface. Since outer-sphere complex formations in general are much faster, an outer-sphere complexation is unlikely. Further studies should be made on the rate in order to as well investigate the pore structure of the material, which could have an effect on the sorption kinetics.

3.2 Optimization of the slag

3.2.1 Visual aspects of the slag

As mentioned, the 61 slag is of high interest since it is the most generated type. And since the t-test comparison between 61L versus 61V showed the highest adsorption capacity of 61V the optimization was focused on this type. Compared to the original slag, the optimized slag showed less variety in color between individual slag grains, where all slag grains turned dark grey. The change in color due to heat treatment could indicate a difference in the surface composition where new mineral phases are formed, thus possibly changing the sorption characteristics of the slag.

3.2.2 Adsorption test

As illustrated in figure 20, at C_e -values around 200 mg/L the adsorption capacity of the optimized slag is at its maximum. Since the majority of the data points at sorption maximum are within the interval 25-35 mg/L, the sorption capacity is believed to be between these values. The release of fluoride from the optimized slag was not measured.

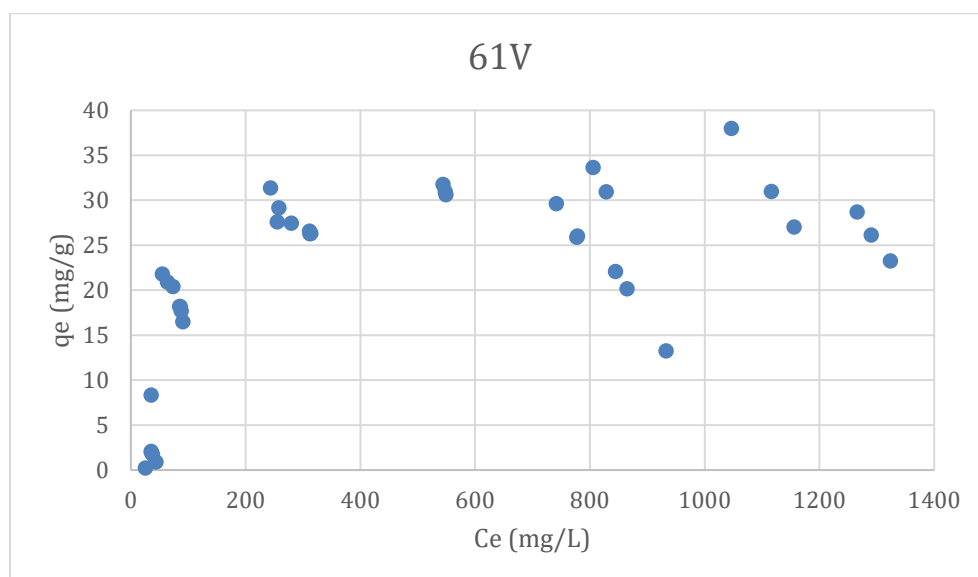


Figure 20. Adsorption of fluoride to the optimized 61V-slag (mg/g) versus concentration of fluoride in the liquid phase.

3.2.3 pH/Conductivity

The pH of the optimized slag samples ended up at higher pH than the original 61V slag, which can be seen in table 31 of the appendix. If the slag contain high abundance of Ca(OH)_2 , water should evaporate when the slag is heated. This would mean that the optimized slag does not contain a high abundance of Ca(OH)_2 . More experiments should therefore be made on the optimized slag in order to investigate the surface composition and what causes to the increase of pH and sorption capacity of fluoride.

Conductivity measurements were not made for the optimized slag samples.

3.2.4 Metals

In the optimized slag samples there were large amounts of aluminum found. During the heating of the optimization process there is likely new mineral phases forming, resulting in more aluminum released from the slag when in aqueous solutions. The high release of aluminum is possibly a factor for the increasing fluoride removal. The reason for this is believed to be a result of a complex formation in the liquid of aluminum fluoride (AlF_3).

The calcium concentrations for the optimized slag had the same trend as the original slag, with a negative correlation between fluoride concentration. Sodium and potassium measurements provided no relevant information regarding the analysis of the slag material. The results from the metal analysis can be found in table 24 of the appendix. Magnesium, iron and manganese were not detected in any of the samples.

3.2.5 Isotherm modeling

In the Sips isotherm modeling for the optimized slag it was not possible to obtain more than one curve. The Q-value (mg/L) obtained from the isotherm was 29.1 mg/g, which is a reasonable value considering at what values most of the q_e -values end up. Further values obtained are $K (\text{L/g}) = 0.0157$, $n = 0.367$, residual sum of squares = 321 and R-squared = 0.893. A reason why the data points are closer to each other and why there is not possible to obtain multiple curves could be due to the visual appearance and the mineral formation during heat treatment. As explained, compared to the original slag there is not as much difference on the optimized slag between slag grains. If heat treating the material makes the slag grains become more similar to each other regarding their sorption characteristics, the samples would not differ as much between each other.

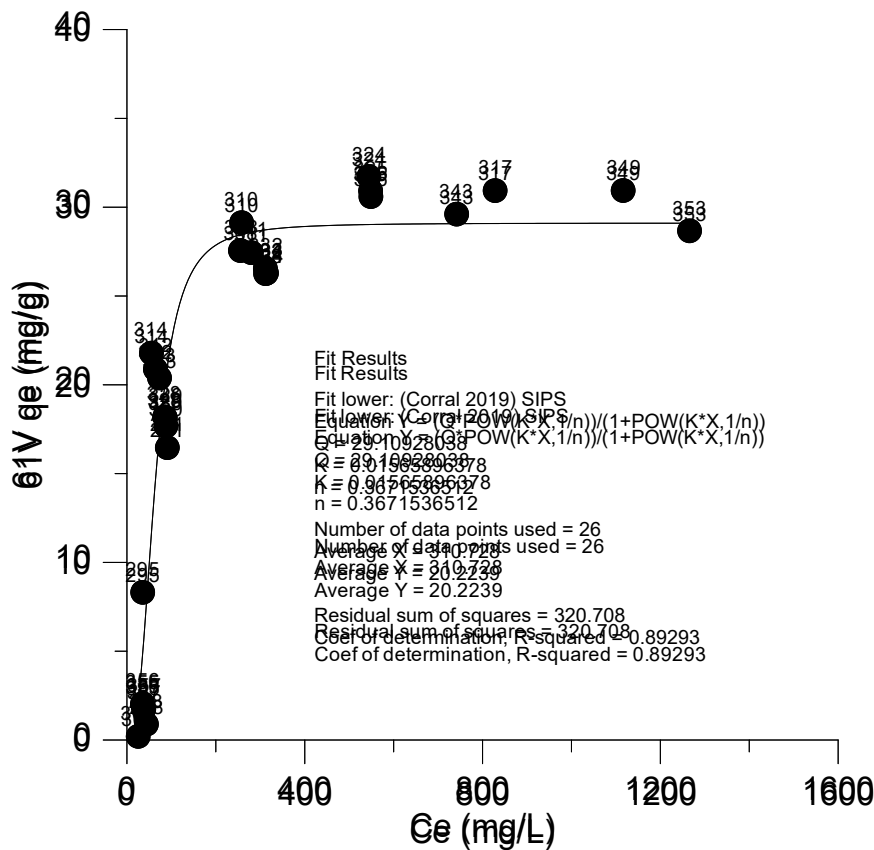


Figure 21. Sips isotherms of the optimized slag.

3.2.6 Kinetics

From the kinetics tests of the optimized 61L-slag, there are indications of a higher adsorption capacity as well as a longer time for the system to reach chemical equilibrium. Instead of an equilibrium time of 3-4 hours, the optimized slag required up to approximately 24 hours with a maximum capacity of around 30 mg/g. These are further indications that there are changes occurring on the slag surface while heating, resulting both a higher sorption capacity as well as longer time for the process to occur. The slower rate of the system could be a result of a change in the pore structure of the slag that occurs during the heat treatment of the slag.

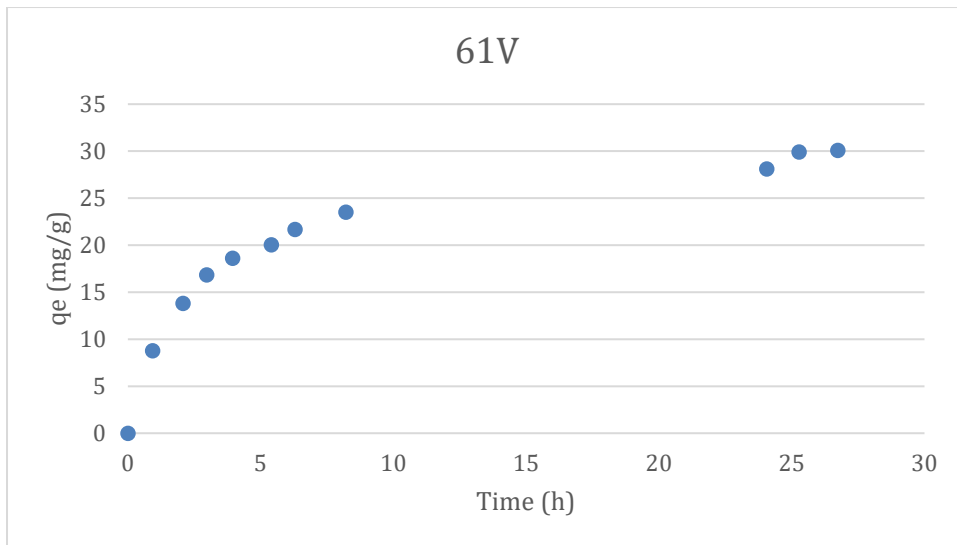


Figure 22. Adsorption of fluoride to optimized 61V-slag (mg/g) versus hours of contact between slag and fluoride solution.

4. Conclusions

In conclusion, AOD-slag works as a treatment of fluoride contaminated waters. Even though there is more regarding the material to be discovered, the results indicate the slag can remove fluoride from aqueous solutions, and that this process can be optimized. It is important to acknowledge that plenty of outliers had to be removed for the isotherm modeling. For this reason there should be more experiments made on the material in order to conclude what parameters that causes the differences between samples, and additionally how to further optimize the method for improved results.

Acknowledgments

I would like to thank my supervisor, Dr. Viktor Sjöberg, for his guidance and helpfulness throughout this project. I would also like to express my gratitude to my family, Dag, Agneta, Lisa and Sara for your love, patience and support.

5. References

- Al-Ghouthi M.A., Da'ana D.A. (2020) *Guidelines for the use and interpretation of adsorption isotherm models: A review*. Journal of Hazard Materials. 2020 Jul 5;393:122383. doi: 10.1016/j.jhazmat.2020.122383.
- Dabrowski A. (2001) *Adsorption--from theory to practice*. Adv Colloid Interface Sci. 2001 Oct 8;93(1-3):135-224. doi: 10.1016/s0001-8686(00)00082-8.
- Del Bello L. (2020) *Fluorosis: an ongoing challenge for India*. Lancet Planet Health. 2020 Mar;4(3):e94-e95. doi: 10.1016/S2542-5196(20)30060-7
- Dolganov, A. V., Revin, V. D., Kostyukov, S. G., Revin, V. V., & Yang, G. (2021). *Kinetic and Thermodynamic Characteristics of Fluoride Ions Adsorption from Solution onto the Aluminum Oxide Nanolayer of a Bacterial Cellulose-Based Composite Material*. Polymers, 13(19), 3421. <https://doi.org/10.3390/polym13193421>
- Foo K.Y., and Hameed B.H. (2009) *Insights into the modeling of adsorption isotherm systems*. Chemical Engineering Journal 156 (2010)
- Habuda-Stanić, M., Ravančić, M. E., & Flanagan, A. (2014). *A Review on Adsorption of Fluoride from Aqueous Solution*. Materials (Basel, Switzerland), 7(9), 6317–6366. <https://doi.org/10.3390/ma7096317>
- IPCS (2002) *Fluoride*. Geneva, World Health Organization, International Programme on Chemical Safety (Environmental Health Criteria 227) https://apps.who.int/iris/bitstream/handle/10665/42415/WHO_EHC_227.pdf?sequence=1&isAllowed=y
- Jernkontoret (2018) *Stålindustrin gör mer än stål. Handbok för restprodukter 2018*. Jernkontoret, Stockholm (2018). <https://www.jernkontoret.se/globalassets/publicerat/handbocker/handbok-for-restprodukter-2018.pdf>
- Khairnar M.R., Dodamani A.S., Jadhav H.C., Naik R.G., Deshmukh M.A. *Mitigation of Fluorosis - A Review*. J Clin Diagn Res. 2015 Jun;9(6):ZE05-9. doi: 10.7860/JCDR/2015/13261.6085
- Lee J.,I., Hong S.H., Lee C.G., Park S.J. (2021) *Fluoride removal by thermally treated egg shells with high adsorption capacity, low cost, and easy acquisition*. Environmental Science and Pollution Research (2021) 28:

- Li J., Liu B., Zeng Y., Wang Z., Gao Z. (2016) *Maximum availability and mineralogical control of chromium released from AOD slag*. Environ Monit Assess (2017) 189:113
- Muhammad K.S., Jun Young K., Young-Gyun C. (2019) *Synthesis of bone char from cattle bones and its application for fluoride removal from the contaminated water*. Groundwater for Sustainable Development. 2019, Volume 8, Pages 324-331.
- Patel R.K., Kumar S., Chawla A.K., Mondal P., Singh N., Teychene B., Pandey J.K. (2018) *Elimination of Fluoride, Arsenic, and Nitrate from Water Through Adsorption onto Nano-adsorbent: A Review*. Current Nanoscience 15 (2019)
- Sivasankar V., Muruges S., Rajkumar S., Darchen A. (2013) *Cerium dispersed in carbon (CeDC) and its adsorption behavior: A first example of tailored adsorbent for fluoride removal from drinking water*. Chemical Engineering Journal. 2013, Volume 214, Pages 45-54. DOI: <https://www.sciencedirect.com/science/article/pii/S1385894712013605?via%3Dihub>
- Strawn D.G., Bohn H.L., O'Connor G.A., (2015) *Soil Chemistry*. Somerset: John Wiley & Sons, Ltd
- Wang J, Guo X. (2020) *Adsorption isotherm models: Classification, physical meaning, application and solving method*. Chemosphere. 2020 Nov;258:127279. doi: 10.1016/j.chemosphere.2020.127279. Epub 2020 Jun 10. PMID: 32947678.
- Wang Y.J., Zeng Y.N., Li J.G., Zhang Y.Z., Zhang Y.J., Zhao Q.Z. (2019) *Carbonation of argon oxygen decarburization stainless steel slag and its effect on chromium leachability*. Journal of Cleaner Production 256 (2020)
- Wu J., Wang T., Shi N., Pan W.P. (2022) *Insight into mass transfer mechanism and equilibrium modeling of heavy metals adsorption on hierarchically porous biochar*. Separation and Purification Technology. Volume 287, 15 April 2022,
- WHO (2006). *Fluoride in Drinking-water*. by. Fawell J., Bailey K., Chilton J., Dahi E., Fewtrell L. and Magara Y. IWA Publishing, London,

APPENDIX

Table 4. Slag information of 38L.

Sample	Slag weight (g)	Start of adsorption test	Time of adsorption test (h)
37	0.2067	09-feb	21.5
44	0.2027	10-feb	18.5
51	0.2019	10-feb	18.5
58	0.2021	11-feb	67.5
65	0.2037	11-feb	68.0
72	0.2025	14-feb	19.0
79	0.2027	14-feb	19.0
86	0.2022	15-feb	19.5
93	0.2022	15-feb	19.5
100	0.1969	16-feb	18.5
107	0.2008	16-feb	19.0
114	0.2034	17-feb	19.0
121	0.2049	17-feb	19.5
128	0.2035	20-feb	19.0
135	0.2036	20-feb	19.5
142	0.1992	21-feb	19.5
149	0.1991	21-feb	19.5
156	0.2020	22-feb	19.0
163	0.2006	22-feb	19.0
170	0.1992	23-feb	19.5
177	0.2036	23-feb	19.5
184	0.1980	24-feb	18.0
191	0.2032	24-feb	18.0
198	0.1954	27-feb	18.5

205	0.2015	27-feb	18.5
212	0.1969	28-feb	19.0
219	0.2019	28-feb	19.5
226	0.1999	01-mars	19.0
233	0.2041	01-mars	19.0
240	0.1988	02-mars	19.0
247	0.1964	02-mars	19.0
254	0.1993	03-mars	19.0
261	0.1959	03-mars	19.0

Table 5. Slag information of 38V.

Sample	Slag weight (g)	Start of adsorption test	Time of adsorption test (h)
38	0.2005	09-feb	21.5
45	0.1965	10-feb	18.5
52	0.1967	10-feb	18.5
59	0.2001	11-feb	67.5
66	0.2011	11-feb	68.0
73	0.2040	14-feb	19.0
80	0.2039	14-feb	19.0
87	0.1969	15-feb	19.5
94	0.1969	15-feb	19.5
101	0.2026	16-feb	18.5
108	0.2049	16-feb	19.0
115	0.1975	17-feb	19.0
122	0.2011	17-feb	19.5
129	0.2037	20-feb	19.0
136	0.2009	20-feb	19.5

143	0.1998	21-feb	19.5
150	0.1991	21-feb	19.5
157	0.1975	22-feb	19.0
164	0.2038	22-feb	19.0
171	0.2035	23-feb	19.5
178	0.2020	23-feb	19.5
185	0.1995	24-feb	18.0
192	0.1952	24-feb	18.0
199	0.1970	27-feb	18.5
206	0.1986	27-feb	18.5
213	0.1991	28-feb	19.0
220	0.2022	28-feb	19.5
227	0.1982	01-mars	19.0
234	0.2006	01-mars	19.0
241	0.1957	02-mars	19.0
248	0.1975	02-mars	19.0
255	0.1964	03-mars	19.0
262	0.1993	03-mars	19.0

Table 6. Slag information of 61L.

Sample	Slag weight (g)	Start of adsorption test	Time of adsorption test (h)
40	0.2012	09-feb	21.5
47	0.2016	10-feb	18.5
54	0.1959	10-feb	18.5
61	0.2039	11-feb	67.5
68	0.1974	11-feb	68.0
75	0.2010	14-feb	19.0

82	0.2061	14-feb	19.0
89	0.2012	15-feb	19.5
96	0.2010	15-feb	19.5
103	0.1953	16-feb	18.5
110	0.1996	16-feb	19.0
117	0.1969	17-feb	19.0
124	0.1996	17-feb	19.5
131	0.2031	20-feb	19.0
138	0.1997	20-feb	19.5
145	0.1973	21-feb	19.5
152	0.1988	21-feb	19.5
159	0.1991	22-feb	19.0
166	0.2048	22-feb	19.0
173	0.1971	23-feb	19.5
180	0.2007	23-feb	19.5
187	0.1954	24-feb	18.0
194	0.1976	24-feb	18.0
201	0.1994	27-feb	18.5
208	0.2008	27-feb	18.5
215	0.2025	28-feb	19.0
222	0.1983	28-feb	19.5
229	0.1969	01-mars	19.0
236	0.2031	01-mars	19.0
243	0.1998	02-mars	19.0
250	0.2022	02-mars	19.0
257	0.1996	03-mars	19.0
264	0.1998	03-mars	19.0

Table 7. Slag information of 61V.

Sample	Slag weight (g)	Start of adsorption test	Time of adsorption test (h)
39	0.2036	09-feb	21.5
46	0.1960	10-feb	18.5
53	0.2030	10-feb	18.5
60	0.2027	11-feb	67.5
67	0.2058	11-feb	68.0
74	0.1985	14-feb	19.0
81	0.1972	14-feb	19.0
88	0.1950	15-feb	19.5
95	0.2024	15-feb	19.5
102	0.1988	16-feb	18.5
109	0.2025	16-feb	19.0
116	0.1966	17-feb	19.0
123	0.1968	17-feb	19.5
130	0.1995	20-feb	19.0
137	0.2011	20-feb	19.5
144	0.1972	21-feb	19.5
151	0.1954	21-feb	19.5
158	0.1983	22-feb	19.0
165	0.1963	22-feb	19.0
172	0.1989	23-feb	19.5
179	0.1973	23-feb	19.5
186	0.2029	24-feb	18.0
193	0.1966	24-feb	18.0
200	0.1971	27-feb	18.5
207	0.1993	27-feb	18.5

214	0.1976	28-feb	19.0
221	0.1991	28-feb	19.5
228	0.1958	01-mars	19.0
235	0.1979	01-mars	19.0
242	0.1981	02-mars	19.0
249	0.1998	02-mars	19.0
256	0.1994	03-mars	19.0
263	0.1990	03-mars	19.0

Table 8. Slag information of 71L.

Sample	Slag weight (g)	Start of adsorption test	Time of adsorption test (h)
41	0.1945	09-feb	21.5
48	0.2041	10-feb	18.5
55	0.2005	10-feb	18.5
62	0.2041	11-feb	67.5
69	0.1971	11-feb	68.0
76	0.1976	14-feb	19.0
83	0.2008	14-feb	19.0
90	0.2037	15-feb	19.5
97	0.1961	15-feb	19.5
104	0.2028	16-feb	18.5
111	0.2017	16-feb	19.0
118	0.2027	17-feb	19.0
125	0.2040	17-feb	19.5
132	0.2047	20-feb	19.0
139	0.2014	20-feb	19.5
146	0.1974	21-feb	19.5

153	0.2030	21-feb	19.5
160	0.2008	22-feb	19.0
167	0.1956	22-feb	19.0
174	0.1995	23-feb	19.5
181	0.1957	23-feb	19.5
188	0.2008	24-feb	18.0
195	0.1993	24-feb	18.0
202	0.2027	27-feb	18.5
209	0.2018	27-feb	18.5
216	0.1989	28-feb	19.0
223	0.1964	28-feb	19.5
230	0.1968	01-mars	19.0
237	0.1957	01-mars	19.0
244	0.2007	02-mars	19.0
251	0.1976	02-mars	19.0
258	0.1973	03-mars	19.0
265	0.1984	03-mars	19.0

Table 9. Slag information of 71V.

Sample	Slag weight (g)	Start of adsorption test	Time of adsorption test (h)
42	0.2004	09-feb	21.5
49	0.2001	10-feb	18.5
56	0.1999	10-feb	18.5
63	0.1993	11-feb	67.5
70	0.2014	11-feb	68.0
77	0.2056	14-feb	19.0
84	0.2048	14-feb	19.0

91	0.2009	15-feb	19.5
98	0.1987	15-feb	19.5
105	0.2030	16-feb	18.5
112	0.2021	16-feb	19.0
119	0.2002	17-feb	19.0
126	0.1989	17-feb	19.5
133	0.2013	20-feb	19.0
140	0.2023	20-feb	19.5
147	0.2019	21-feb	19.5
154	0.1979	21-feb	19.5
161	0.2007	22-feb	19.0
168	0.2020	22-feb	19.0
175	0.1974	23-feb	19.5
182	0.1977	23-feb	19.5
189	0.2037	24-feb	18.0
196	0.2016	24-feb	18.0
203	0.1988	27-feb	18.5
210	0.1978	27-feb	18.5
217	0.1965	28-feb	19.0
224	0.1969	28-feb	19.5
231	0.1961	01-mars	19.0
238	0.1968	01-mars	19.0
245	0.1997	02-mars	19.0
252	0.1994	02-mars	19.0
259	0.2001	03-mars	19.0
266	0.2000	03-mars	19.0

Table 10. Slag information of optimized 61V.

Sample	Slag weight (g)	Start of adsorption test	Time of adsorption test (h)
291	0.2030	22-mars	19.5
295	0.2018	24-mars	21.5
298	0.1966	24-mars	21.5
301	0.2008	25-mars	23.0
306	0.1977	31-mars	21.5
307	0.1976	31-mars	21.5
308	0.1985	31-mars	21.5
309	0.1955	31-mars	21.5
310	0.2005	31-mars	21.5
311	0.1969	31-mars	21.5
312	0.2010	31-mars	21.5
313	0.1970	31-mars	21.5
314	0.2006	31-mars	21.5
316	0.1990	11-apr	25.5
317	0.2016	11-apr	25.5
324	0.1957	11-apr	25.5
325	0.1982	11-apr	25.5
326	0.1999	11-apr	25.5
328	0.1987	12-apr	25.5
329	0.1976	12-apr	25.5
330	0.2010	12-apr	25.5
332	0.1983	12-apr	25.5
333	0.2001	12-apr	25.5
334	0.1984	12-apr	25.5
343	0.1989	20-apr	25.5
344	0.1985	20-apr	25.5

345	0.2002	20-apr	25.5
347	0.2004	20-apr	25.5
348	0.1986	20-apr	25.5
349	0.1985	20-apr	25.5
351	0.1973	21-apr	25.5
352	0.2010	21-apr	25.5
353	0.2003	21-apr	25.5
355	0.2003	21-apr	25.5
356	0.1991	21-apr	25.5
357	0.2025	21-apr	25.5
358	0.2034	21-apr	25.5

Table 11. Results from the IC analysis of 38L.

Sample	Ci (mg/L)	Ce (mg/L)	qe (mg/g)
37	100.6947877	94.42291133	0.6068578967
44	144.4008553	108.7827946	3.514362180
51	299.639773	180.8512213	11.76706802
58	332.6832734	363.4397726	-3.043691163
65	602.4120000	467.8207807	13.21465088
72	230.0870518	207.7358639	2.207524728
79	377.1730516	347.8656088	2.891706246
86	30.00625427	33.33074232	-0.3288316572
93	474.6401877	400.7331911	7.310286507
100	62.81031428	55.77803424	0.714299649
107	835.7813644	791.0492292	4.455391957
114	149.3691591	131.3764711	1.769192529
121	363.0265494	315.2044742	4.667845311

128	246.8404772	222.8217299	2.360564849
135	1090.244823	1022.558415	6.648959546
142	956.7317196	799.3885585	15.79750613
149	1403.821091	1346.554988	5.752496503
156	2274.855289	2426.591826	-15.02341955
163	4931.968076	4650.66655	28.04601456
170	7463.071292	7414.953809	4.831072591
177	10270.16559	10092.37232	17.46495793
184	2985.347198	2930.056561	5.584912825
191	3960.103550	3917.291159	4.213818034
198	5880.150685	5801.273973	8.073358478
205	7024.077626	6853.392694	16.94143241
212	7983.431885	8141.624325	-16.06830274
219	9098.356201	8939.730017	15.71334165
226	2073.686033	1916.650792	15.71137980
233	3809.013767	3865.321673	-5.517678143
240	4604.983132	4336.703658	26.98988676
247	6439.571200	6422.001953	1.789129039
254	8316.315698	7841.646363	47.63365130
261	9717.934215	9595.762269	12.47288879

Table 12. Obtained results from the IC analysis of 38V.

Sample	Ci (mg/L)	Ce (mg/L)	qe (mg/g)
38	100.6947877	-	-
45	144.4008553	129.6685583	1.499470439
52	299.6397730	186.2357102	11.53066221
59	332.6832734	369.4650171	-3.676336203

66	602.4120000	453.6487503	14.79495273
73	230.0870518	182.6933462	4.646441727
80	377.1730516	324.6973788	5.147196943
87	30.00625427	28.66265358	0.1364754380
94	474.6401877	386.9900171	8.903013778
101	62.81031428	51.30320245	1.135943912
108	835.7813644	785.9389319	4.865049537
115	149.3691591	129.3822162	2.023994217
122	363.0265494	286.6076776	7.600086710
129	246.8404772	218.1953984	2.812477057
136	1090.244823	979.2520665	11.04955268
143	956.7317196	754.1552894	20.27792094
150	1403.821091	1367.419382	3.656625684
157	2274.855289	2198.561656	7.725937488
164	4931.968076	4610.936678	31.50455329
171	7463.071292	7449.492766	1.334498807
178	10270.16559	10126.36221	14.23795857
185	2985.347198	2912.365994	7.316411460
192	3960.10355	4161.782979	-20.66387594
199	5880.150685	5770.515982	11.13042672
206	7024.077626	7042.068493	-1.811769142
213	7983.431885	7876.757546	10.71565428
220	9098.356201	8862.736125	23.30564551
227	2073.686033	1961.962075	11.27386062
234	3809.013767	3644.047104	16.44732440
241	4604.983132	4296.149680	31.56192659
248	6439.571200	6385.878018	5.437284235

255	8316.315698	8236.477550	8.130157666
262	9717.934215	9597.154542	12.12038864

Table 13. Obtained results from the IC analysis of 61L.

Sample	Ci (mg/L)	Ce (mg/L)	qe (mg/g)
40	100.6947877	105.1170281	-0.4395865172
47	144.4008553	130.7928284	1.350002676
54	299.6397730	284.8112509	1.513886889
61	332.6832734	370.6428153	-3.723348889
68	602.4120000	500.0760679	10.36838218
75	230.0870518	205.0462874	2.491618353
82	377.1730516	349.9643202	2.640342696
89	30.00625427	31.38304608	-0.1368580327
96	474.6401877	424.9985495	4.939466490
103	62.81031428	65.92146325	-0.3186020446
110	835.7813644	789.6157908	4.625808981
117	149.3691591	146.6872302	0.2724153350
124	363.0265494	327.5329909	3.556468787
131	246.8404772	228.0224116	1.853083763
138	1090.244823	1011.693481	7.866934616
145	956.7317196	879.4555658	7.833365817
152	1403.821091	1430.975794	-2.731861476
159	2274.855289	2293.281880	-1.850988631
166	4931.968076	4929.784248	0.2132643940
173	7463.071292	7355.253617	10.94040332
180	10270.16559	10541.38748	-27.02759272
187	2985.347198	2924.026279	6.276450246

194	3960.103550	3909.007135	5.171701913
201	5880.150685	5755.319635	12.52066702
208	7024.077626	6836.908676	18.64232567
215	7983.431885	8148.050810	-16.25865930
222	9098.356201	8984.786226	11.45435949
229	2073.686033	1892.666032	18.38699865
236	3809.013767	3816.070655	-0.6949175817
243	4604.983132	4476.964666	12.81466125
250	6439.571200	6416.044922	2.327030505
257	8316.315698	8404.968674	-8.883063726
264	9717.934215	9862.295510	-14.45058006

Table 14. Obtained results from the IC analysis of 61V.

Sample	Ci (mg/L)	Ce (mg/L)	qe (mg/g)
39	100.6947877	83.39532335	1.699357991
46	144.4008553	100.9778765	4.430916211
53	299.639773	263.8621597	3.524888009
60	332.6832734	337.9219259	-0.516887273
67	602.412	424.3659617	17.30282199
74	230.0870518	181.5028491	4.895133772
81	377.1730516	343.264925	3.438958072
88	30.00625427	27.47988908	0.259114378
95	474.6401877	406.7417235	6.709334404
102	62.81031428	50.42363512	1.246144785
109	835.7813644	760.8039349	7.405178224
116	149.3691591	115.1917566	3.476846644
123	363.0265494	274.5759923	8.988877754

130	246.8404772	206.5388155	4.040266837
137	1090.244823	954.0539412	13.54459294
144	956.7317196	697.0818326	26.33365993
151	1403.821091	1367.804674	3.686429558
158	2274.855289	2258.875636	1.611664417
165	4931.968076	4781.634801	15.31668618
172	7463.071292	7368.858288	9.473404053
179	10270.16559	10191.81454	7.942326869
186	2985.347198	2973.373651	1.180241184
193	3960.10355	4033.894013	-7.506659505
200	5880.150685	6009.319635	-13.10694569
207	7024.077626	6958.552511	6.575525756
214	7983.431885	7924.619811	5.952639069
221	9098.356201	8929.550323	16.95689379
228	2073.686033	1889.081306	18.85645839
235	3809.013767	3760.221664	4.930985671
242	4604.983132	4357.21147	25.01480686
249	6439.5712	6109.55522	33.03463264
256	8316.315698	8224.434389	9.215778208
263	9717.934215	9109.684998	61.13057456

Table 15. Obtained results from the IC analysis of 71L.

Sample	Ci (mg/L)	Ce (mg/L)	qe (mg/g)
41	100.6947877	91.91930488	0.9023632720
48	144.4008553	93.68327987	4.969875106
55	299.6397730	265.8804178	3.367516729
62	332.6832734	354.7989635	-2.167142582

69	602.4120000	478.3908719	12.58458936
76	230.0870518	171.2117998	5.959033607
83	377.1730516	353.8803366	2.319991534
90	30.00625427	31.10284130	−0.1076668660
97	474.6401877	458.0326792	1.693779555
104	62.81031428	54.13711779	0.855344822
111	835.7813644	842.1649774	−0.6329809599
118	149.3691591	123.7189154	2.530857793
125	363.0265494	322.7436455	3.949304304
132	246.8404772	225.1847465	2.115850583
139	1090.244823	996.9342139	9.266197546
146	956.7317196	851.7941201	10.63197563
153	1403.821091	1422.155959	−1.806391026
160	2274.855289	2207.849500	6.673883313
167	4931.968076	4922.820558	0.9353290370
174	7463.071292	7575.194352	−11.24040710
181	10270.16559	10166.45285	10.59915604
188	2985.347198	2947.129307	3.806562819
195	3960.103550	4086.304386	−12.66440897
202	5880.150685	5872.09589	0.7947503230
209	7024.077626	7225.474886	−19.96008526
216	7983.431885	7977.235549	0.6230603630
223	9098.356201	8939.818536	16.14436506
230	2073.686033	1949.657979	12.60447707
237	3809.013767	3784.197766	2.536126866
244	4604.983132	4507.220348	9.742180776
251	6439.571200	6643.566229	−20.64727008

258	8316.315698	8482.413853	-16.83711660
265	9717.934215	9594.369997	12.45607042

Table 16. Obtained results from the IC analysis of 71V.

Sample	Ci (mg/L)	Ce (mg/L)	qe (mg/g)
42	100.6947877	103.6685193	-0.2967795998
49	144.4008553	112.0700716	3.231462647
56	299.6397730	259.0986101	4.056144365
63	332.6832734	328.1476218	0.4551582130
70	602.4120000	393.1739530	20.77835620
77	230.0870518	182.2295959	4.655394547
84	377.1730516	336.7005348	3.952394226
91	30.00625427	26.70633959	0.3285131580
98	474.6401877	432.2587884	4.265868074
105	62.81031428	55.27339239	0.7425538820
112	835.7813644	746.6279704	8.822701048
119	149.3691591	128.5996605	2.074874986
126	363.0265494	320.8346971	4.242519092
133	246.8404772	214.9469962	3.168751221
140	1090.244823	937.7437580	15.07672419
147	956.7317196	780.7940364	17.42820042
154	1403.821091	1382.780802	2.126355546
161	2274.855289	2170.873531	10.36190908
168	4931.968076	5020.899842	-8.805125382
175	7463.071292	7529.081401	-6.687954388
182	10270.16559	10214.91023	5.589818912
189	2985.347198	2958.180473	2.667326920
196	3960.103550	3879.795510	7.967067498

203	5880.150685	5793.876712	8.679474105
210	7024.077626	6719.484018	30.79814027
217	7983.431885	7867.020448	11.84849228
224	9098.356201	9027.009826	7.246965479
231	2073.686033	1935.890553	14.05359308
238	3809.013767	3691.375877	11.95507020
245	4604.983132	4485.229936	11.99330957
252	6439.571200	6328.678089	11.12267912
259	8316.315698	8225.095719	9.117439192
266	9717.934215	9597.241559	12.06926558

Table 17. Obtained results from the IC analysis of optimized 61V.

Sample	Ci (mg/L)	Ce (mg/L)	qe (mg/g)
291	266.4506585	90.8385497	16.4798555
295	118.4990949	35.4442982	8.33428957
298	52.69043936	43.7990456	0.909038730
301	27.57146325	25.3205843	0.224751610
306	1063.698789	932.673744	13.2549363
307	1063.698789	864.605241	20.1511688
308	1063.698789	844.476696	22.0878683
309	550.1532592	243.542710	31.3668081
310	550.1532592	257.947255	29.1477311
311	550.1532592	279.806601	27.4603004
312	279.4267706	64.0625311	20.8935456
313	279.4267706	73.2836291	20.4050318
314	279.4267706	55.1233206	21.8041739
316	1140.269991	805.449840	33.6502663
317	1140.269991	828.266195	30.9527575

324	847.3186406	544.252998	31.7467843
325	847.3186406	548.187268	30.9394205
326	847.3186406	548.779867	30.6155320
328	261.3627460	84.8271748	18.2132824
329	261.3627460	86.2538510	18.1666617
330	261.3627460	87.7806073	17.7036510
332	574.8245926	311.360075	26.5723165
333	574.8245926	311.919241	26.2773964
334	574.8245926	313.856736	26.3072436
343	1036.378710	741.718621	29.6289683
344	1036.378710	778.123860	26.0206398
345	1036.378710	777.169624	25.8950136
347	1417.609020	1046.36047	37.9770222
348	1417.609020	1155.74532	27.0302414
349	1417.609020	1116.33228	30.9582612
351	1552.972383	1323.45001	23.2663325
352	1552.972383	1290.30975	26.1355858
353	1552.972383	1265.64761	28.6894430
355	54.77713422	35.8776966	1.98146874
356	54.77713422	35.1379166	2.07143933
357	54.77713422	37.8097037	1.75958539
358	522.4146730	255.306472	27.5775429

Table 18. Results from the metal analysis of 38L.

Sample	Ca (ppm)	Al (ppm)	Na (ppm)	K (ppm)
37	25.0	27.5	118.0	1.0
44	10.5	21.5	170.5	0.0

51	4.00	17.5	253.5	0.0
58	5.00	10.0	468.0	0.0
65	3.50	8.00	585.5	0.0
72	13.0	12.5	276.5	0.0
79	2.50	8.00	443.0	-1.0
86	334	187	393.0	1.0
93	1.50	6.00	525.5	1.0
100	215	171	752.5	4.0
107	0.500	5.00	889.0	1.5
114	48.0	175	1712	5.0
121	3.00	10.5	423.0	0.0
128	3.50	17.5	324.5	2.0
135	0.500	5.00	1113	2.0
142	0.500	4.00	1007	2.0
149	1.00	5.00	N/A*	2.0
156	1.00	3.50	N/A	0.0
163	0.500	1.50	N/A	1.0
170	0.500	0.00	N/A	3.0
177	1.50	1.00	N/A	7.0
184	3.00	30.5	N/A	3.0
191	2.00	12.5	N/A	2.5
198	2.50	11.0	N/A	2.0
205	1.50	1.00	N/A	3.0
212	<LOQ	1.00	N/A	3.0
219	1.50	0.00	N/A	4.5
233	<LOQ	16.0	N/A	3.0
240	2.00	17.0	N/A	6.0

247	<LOQ	4.00	N/A	7.5
254	2.00	0.00	N/A	4.5
261	0.500	0.00	N/A	5.0

*concentration too high to be quantified.

Table 19. Results from the metal analysis of 38V.

Sample	Ca (ppm)	Al (ppm)	Na (ppm)	K (ppm)
38	12.5	6.00	112.0	2.0
45	6.50	4.50	197.5	1.0
52	4.50	6.00	264.5	0.0
59	7.50	5.00	534.5	2.0
66	8.50	4.00	620.5	1.0
73	6.00	6.00	254.0	-1.0
80	3.50	5.00	450.5	0.0
87	180	37.5	441.5	2.0
94	2.50	4.50	557.5	2.0
101	111	43.5	731.0	2.5
108	0.50	6.00	977.0	3.0
115	74.5	65.0	1644	0.0
122	4.50	5.00	409.5	1.0
129	4.00	4.50	309.5	3.0
136	0.50	5.00	1116	2.0
143	1.00	5.00	930.5	2.0
150	1.00	8.00	N/A*	2.0
157	1.00	8.00	N/A	0.0
164	0.50	5.00	N/A	0.0
171	<LOQ	23.0	N/A	4.0
178	<LOQ	8.00	N/A	7.5

185	2.50	80.0	N/A	3.0
192	<LOQ	65.5	N/A	4.0
199	<LOQ	59.5	N/A	3.5
206	<LOQ	32.5	N/A	4.0
213	<LOQ	15.5	N/A	3.5
220	<LOQ	14.5	N/A	5.0
227	3.00	85.0	N/A	2.0
234	1.50	85.5	N/A	4.0
241	<LOQ	61.5	N/A	5.5
248	0.500	39.0	N/A	8.5
255	<LOQ	11.0	N/A	4.0
262	<LOQ	6.50	N/A	4.5

*concentration too high to be quantified.

Table 20. Results from the metal analysis of 61L.

Sample	Ca (ppm)	Al (ppm)	Na (ppm)	K (ppm)
40	9.50	5.00	126.0	2.0
47	16.0	3.00	196.5	1.0
54	2.00	3.00	389.5	1.0
61	6.00	4.00	516.0	1.0
68	1.50	5.00	646.0	1.0
75	3.00	3.00	277.5	0.0
82	2.00	3.00	474.0	0.0
89	103	47.5	439.0	2.0
96	1.50	4.00	569.0	2.0
103	53.5	38.5	880.0	3.0
110	1.50	5.00	1006	3.0
117	40.0	29.0	1807	1.0

124	2.00	3.00	451.0	1.0
131	3.50	3.00	330.0	3.0
138	0.500	5.00	1217	4.0
145	0.500	3.50	986.0	2.0
152	1.00	5.00	N/A*	2.0
159	1.00	4.50	N/A	1.0
166	0.500	2.00	N/A	1.0
173	0.00	7.00	N/A	4.0
180	<LOQ	0.00	N/A	6.0
187	1.50	32.5	N/A	2.5
194	1.00	22.5	N/A	3.0
201	1.00	10.0	N/A	3.0
208	0.500	8.50	N/A	3.0
215	<LOQ	5.00	N/A	3.0
222	<LOQ	1.00	N/A	4.0
229	1.00	47.5	N/A	2.0
236	<LOQ	29.5	N/A	3.0
243	2.00	17.5	N/A	6.0
250	<LOQ	9.00	N/A	6.5
257	<LOQ	1.00	N/A	4.0
264	<LOQ	1.00	N/A	4.5

*concentration too high to be quantified.

Table 21. Results from the metal analysis of 61V.

Sample	Ca (ppm)	Al (ppm)	Na (ppm)	K (ppm)
39	26.0	33.5	121.5	2.0
46	12.0	26.5	189.5	1.0
53	4.00	14.0	399.5	1.0

60	9.50	8.00	520.0	1.0
67	11.0	5.00	607.0	2.0
74	5.50	20.0	290.0	0.0
81	3.00	8.00	478.0	0.0
88	519	312	475.0	4.5
95	3.50	7.00	571.5	2.0
102	283	260	798.5	3.0
109	2.00	4.00	1009	4.0
116	79.0	273	1850	2.0
123	3.50	10.0	413.0	1.0
130	5.50	17.0	317.0	3.0
137	1.50	5.00	1181	4.0
144	1.50	4.00	905.5	2.0
151	1.00	7.00	N/A*	1.0
158	1.00	7.00	N/A	1.0
165	0.50	8.00	N/A	1.0
172	<LOQ	64.0	N/A	5.5
179	<LOQ	34.5	N/A	7.5
186	<LOQ	104	N/A	4.0
193	0.50	81.0	N/A	4.0
200	<LOQ	73.5	N/A	4.0
207	0.00	77.5	N/A	5.0
214	<LOQ	51.0	N/A	4.0
221	<LOQ	53.5	N/A	6.5
235	1.00	101	N/A	5.0
242	1.00	100	N/A	7.5
249	1.00	66.5	N/A	8.0

256	<LOQ	53.0	N/A	6.0
263	<LOQ	21.5	N/A	7.0

*concentration too high to be quantified.

Table 22. Results from the metal analysis of 71L.

Sample	Ca (ppm)	Al (ppm)	Na (ppm)	K (ppm)
41	31.0	33.0	120.0	2
48	11.0	28.0	156.5	2
55	2.50	17.5	371.5	1
62	4.00	11.5	461.5	1
69	2.00	10.0	617.0	2
76	6.00	22.0	271.0	1
83	1.50	12.5	473.0	0
90	375	219	421.0	2
97	1.50	8.50	590.0	2
104	254	253	807.0	3
111	1.50	8.00	1005	3
118	73.0	294	1845	2
125	2.00	17.0	443.5	3
132	3.50	24.5	319.0	3
139	0.500	5.00	1138	3
146	0.500	6.50	926.0	3
153	0.500	7.00	N/A*	2
160	1.00	7.00	N/A	0
167	0.500	2.00	N/A	1
174	<LOQ	2.00	N/A	4
181	<LOQ	2.00	N/A	5
188	2.50	33.0	N/A	3

195	<LOQ	20.0	N/A	2
202	<LOQ	12.0	N/A	2
209	<LOQ	2.00	N/A	3
216	<LOQ	1.00	N/A	4
223	<LOQ	1.00	N/A	4
230	3.00	66.0	N/A	2
237	1.50	21.0	N/A	3
244	0.500	24.0	N/A	5
251	1.00	6.50	N/A	6
258	<LOQ	1.00	N/A	4
265	<LOQ	1.00	N/A	4

*concentration too high to be quantified.

Table 23. Results from the metal analysis of 71V.

Sample	Ca (ppm)	Al (ppm)	Na (ppm)	K (ppm)
42	27.5	3.00	117.0	2.0
49	15.0	7.00	179.5	2.0
56	7.00	7.00	371.0	1.0
63	11.0	6.00	458.5	2.0
70	10.0	5.00	562.0	1.5
77	9.50	5.50	270.0	0.0
84	7.50	6.00	445.0	1.0
91	398	24.0	400.5	2.0
98	5.00	7.50	624.5	2.0
105	176	39.5	753.0	3.0
112	2.50	5.00	930.0	3.0
119	122	74.0	1740	1.5
126	6.00	6.50	445.0	2.0

133	7.50	9.50	320.5	3.0
140	2.00	5.00	1110	3.5
147	2.50	5.00	N/A*	1.0
154	1.00	5.00	N/A	1.0
161	1.00	6.00	N/A	0.0
168	0.500	7.00	N/A	1.0
175	<LOQ	29.0	N/A	4.0
182	<LOQ	16.0	N/A	7.0
189	<LOQ	66.5	N/A	3.0
196	<LOQ	58.5	N/A	3.0
203	<LOQ	63.0	N/A	4.0
210	<LOQ	51.5	N/A	3.0
217	<LOQ	38.5	N/A	4.0
224	<LOQ	15.5	N/A	4.0
231	4.00	53.5	N/A	2.0
238	1.00	75.5	N/A	3.0
245	0.500	66.5	N/A	4.0
252	0.500	49.0	N/A	6.0
259	<LOQ	20.5	N/A	5.0
266	<LOQ	12.0	N/A	4.0

*concentration too high to be quantified.

Table 24. Results from the metal analysis of optimized 61V.

Sample	Ca (ppm)	Al (ppm)	Na (ppm)	K (ppm)
291	27.5	147.5	311.0	1.0
306	3.00	157.5	1104	4.0
307	4.50	212.5	N/A*	3.0
308	4.00	227.5	N/A	4.5
309	21.0	202.5	617.0	2.0

310	18.0	186.5	644.5	2.0
311	17.0	176.0	643.0	2.0
312	73.0	101.0	361.0	2.0
313	67.0	89.50	362.0	2.0
314	96.0	86.50	363.5	2.0
316	3.00	183.0	N/A	1.0
317	2.50	158.0	977.0	2.5
324	6.00	175.0	869.5	1.0
325	6.00	192.0	932.5	1.0
326	5.50	173.5	861.0	1.0
328	36.5	170.5	308.5	4.0
329	28.5	141.5	306.5	4.0
330	27.0	152.0	316.5	4.0
332	9.00	158.0	600.0	4.5
333	9.50	157.0	591.0	4.0
334	10.0	147.5	612.5	4.0
343	2.50	179.0	1016	1.0
344	3.00	238.5	N/A	2.0
345	2.50	151.0	N/A	1.0
347	2.50	176.5	N/A	6.0
348	2.00	203.0	N/A	2.0
349	1.50	189.0	1277	1.0
351	1.00	165.5	N/A	0.0
352	1.00	173.5	N/A	2.0
353	1.50	220.5	N/A	1.0
355	175	72.50	68.00	1.0
356	225	88.50	71.50	1.0

357	210	69.50	68.50	1.0
358	14.0	182.0	586.0	1.0

*concentration too high to be quantified.

Table 25. pH and conductivity measurements of 38L.

Sample	pH (Ci)	pH (Ce)	EC (Ci) (mS/cm)	EC (Ce) (mS/cm)
37	6.520	9.389	0.6043	0.6043
44	7.004	10.373	0.9018	0.9267
51	6.849	10.431	1.696	1.273
58	7.863	10.794	2.874	2.463
65	6.839	10.797	1.918	2.968
72	6.747	10.337	1.368	1.476
79	8.471	10.506	2.064	1.453
86	8.254	10.112	0.2198	0.4560
93	6.961	9.5130	2.739	2.626
100	9.445	10.289	0.4792	N/A*
107	9.333	10.556	4.348	N/A
114	8.681	10.335	0.9355	N/A
121	8.321	10.603	2.056	N/A
128	8.078	10.559	1.460	N/A
135	9.157	10.348	4.626	N/A
142	8.847	10.428	5.559	N/A
149	9.452	10.447	8.032	N/A
156	9.556	10.532	11.61	N/A
163	9.909	10.826	23.01	N/A
170	9.9	10.852	31.03	N/A
177	10.039	10.683	41.38	N/A

184	9.708	10.599	14.93	N/A
191	9.707	10.605	18.66	N/A
198	9.865	10.816	24.89	N/A
205	9.950	10.725	29.54	N/A
212	9.939	10.652	32.26	N/A
219	10.012	10.730	37.44	N/A
226	9.632	10.476	10.38	N/A
233	9.737	10.588	17.46	N/A
240	9.889	10.725	20.44	N/A
247	10.012	10.832	27.14	N/A
254	10.038	10.666	35.60	N/A
261	10.102	10.693	38.58	N/A

*not measured

Table 26. pH and conductivity measurements of 38V.

Sample	pH (Ci)	pH (Ce)	EC (Ci) (mS/cm)	EC (Ce) (mS/cm)
38	6.520	10.352	0.6043	0.6491
45	7.004	10.632	0.9018	0.9754
52	6.849	10.765	1.696	1.404
59	7.863	11.230	2.874	2.619
66	6.839	11.380	1.918	3.289
73	6.747	10.806	1.368	1.400
80	8.471	10.949	2.064	2.212
87	8.254	10.246	0.2198	0.3765
94	6.961	10.993	2.739	2.643
101	9.445	10.363	0.4792	N/A*
108	9.333	11.126	4.348	N/A

115	8.681	10.708	0.9355	N/A
122	8.321	10.923	2.056	N/A
129	8.078	10.765	1.460	N/A
136	9.157	11.032	4.626	N/A
143	8.847	11.082	5.559	N/A
150	9.452	10.992	8.032	N/A
157	9.556	10.976	11.61	N/A
164	9.909	11.069	23.01	N/A
171	9.900	11.235	31.03	N/A
178	10.04	11.331	41.38	N/A
185	9.708	11.040	14.93	N/A
192	9.707	11.119	18.66	N/A
199	9.865	11.176	24.89	N/A
206	9.950	11.229	29.54	N/A
213	9.939	11.248	32.26	N/A
220	10.01	11.321	37.44	N/A
227	9.632	11.008	10.38	N/A
234	9.737	11.132	17.46	N/A
241	9.889	11.140	20.44	N/A
248	10.01	11.148	27.14	N/A
255	10.03	11.283	35.60	N/A
262	10.10	11.302	38.58	N/A

*not measured

Table 27. pH and conductivity measurements of 61L.

Sample	pH (Ci)	pH (Ce)	EC (Ci) (mS/cm)	EC (Ce) (mS/cm)
40	6.520	9.605	0.6043	0.6386

47	7.004	9.740	0.9018	0.8808
54	6.849	10.077	1.696	1.775
61	7.863	10.838	2.874	2.575
68	6.839	10.533	1.918	2.991
75	6.747	9.9120	1.368	1.395
82	8.471	10.206	2.064	2.273
89	8.254	9.3130	0.2198	0.2842
96	6.961	10.201	2.739	2.632
103	9.445	9.5540	0.4792	0.5165
110	9.333	10.358	4.348	4.427
117	8.681	10.124	0.9355	1.024
124	8.321	10.319	2.056	2.078
131	8.078	10.365	1.460	1.545
138	9.157	10.319	4.626	5.468
145	8.847	10.340	5.559	5.347
152	9.452	10.486	8.032	8.003
159	9.556	10.642	11.61	12.43
166	9.909	10.716	23.01	12.43
173	9.900	10.903	31.03	31.12
180	10.04	10.842	41.38	41.61
187	9.708	10.564	14.93	14.96
194	9.707	10.642	18.66	19.44
201	9.865	10.670	24.89	25.50
208	9.950	10.969	29.54	29.10
215	9.939	10.884	32.26	33.51
222	10.01	10.839	37.44	37.56
229	9.632	10.528	10.38	10.34

236	9.737	10.746	17.46	17.90
243	9.889	10.654	20.44	20.86
250	10.01	10.736	27.14	27.75
257	10.03	10.885	35.60	35.68
264	10.10	10.887	38.58	39.32

Table 28. pH and conductivity measurements of 61V.

Sample	pH (Ci)	pH (Ce)	EC (Ci) (mS/cm)	EC (Ce) (mS/cm)
39	6.520	10.524	0.6043	0.7017
46	7.004	10.823	0.9018	1.052
53	6.849	10.878	1.696	1.850
60	7.863	11.207	2.874	2.753
67	6.839	11.402	1.918	3.405
74	6.747	10.891	1.368	1.448
81	8.471	10.966	2.064	2.305
88	8.254	10.732	0.2198	0.6082
95	6.961	10.961	2.739	2.755
102	9.445	10.768	0.4792	0.6646
109	9.333	11.252	4.348	4.818
116	8.681	10.854	0.9355	1.120
123	8.321	11.006	2.056	2.028
130	8.078	10.986	1.460	1.635
137	9.157	11.383	4.626	5.627
144	8.847	11.340	5.559	5.201
151	9.452	11.329	8.032	8.268
158	9.556	11.312	11.61	12.17

165	9.909	11.328	23.01	22.24
172	9.900	11.377	31.03	31.18
179	10.04	11.448	41.38	40.38
186	9.708	11.349	14.93	14.98
193	9.707	11.235	18.66	19.64
200	9.865	11.343	24.89	25.41
207	9.950	11.394	29.54	28.96
214	9.939	11.384	32.26	33.61
221	10.01	11.435	37.44	36.63
228	9.632	11.278	10.38	10.57
235	9.737	11.318	17.46	18.32
242	9.889	11.329	20.44	20.02
249	10.01	11.366	27.14	27.65
256	10.03	11.410	35.60	34.83
263	10.10	11.348	38.58	38.74

Table 29. pH and conductivity measurements of 71L.

Sample	pH (Ci)	pH (Ce)	EC (Ci) (mS/cm)	EC (Ce) (mS/cm)
41	6.520	10.344	0.6043	0.7258
48	7.004	10.464	0.9018	0.8263
55	6.849	10.370	1.696	1.678
62	7.863	10.774	2.874	2.396
69	6.839	10.670	1.918	2.891
76	6.747	10.546	1.368	1.331
83	8.471	10.437	2.064	2.151
90	8.254	10.170	0.2198	0.4704

97	6.961	10.451	2.739	2.769
104	9.445	10.384	0.4792	N/A*
111	9.333	10.559	4.348	N/A
118	8.681	10.494	0.9355	N/A
125	8.321	10.616	2.056	N/A
132	8.078	10.620	1.460	N/A
139	9.157	10.314	4.626	N/A
146	8.847	10.356	5.559	N/A
153	9.452	10.449	8.032	N/A
160	9.556	10.661	11.61	N/A
167	9.909	10.743	23.01	N/A
174	9.900	10.734	31.03	N/A
181	10.04	10.791	41.38	N/A
188	9.708	10.542	14.93	N/A
195	9.707	10.474	18.66	N/A
202	9.865	10.793	24.89	N/A
209	9.950	10.624	29.54	N/A
216	9.939	10.732	32.26	N/A
223	10.01	10.709	37.44	N/A
230	9.632	10.488	10.38	N/A
237	9.737	10.548	17.46	N/A
244	9.889	10.646	20.44	N/A
251	10.01	10.883	27.14	N/A
258	10.03	10.801	35.60	N/A
265	10.10	10.619	38.58	N/A

*not measured

Table 30. pH and conductivity measurements of 71V.

Sample	pH (Ci)	pH (Ce)	EC (Ci) (mS/cm)	EC (Ce) (mS/cm)
42	6.520	10.355	0.6043	0.822
49	7.004	10.716	0.9018	0.9868
56	6.849	10.982	1.696	1.962
63	7.863	11.214	2.874	2.609
70	6.839	11.380	1.918	3.253
77	6.747	10.816	1.368	1.313
84	8.471	11.066	2.064	2.336
91	8.254	10.826	0.2198	0.6581
98	6.961	11.232	2.739	3.005
105	9.445	10.676	0.4792	0.6601
112	9.333	11.377	4.348	N/A*
119	8.681	10.869	0.9355	N/A
126	8.321	11.058	2.056	N/A
133	8.078	10.958	1.460	N/A
140	9.157	11.342	4.626	N/A
147	8.847	11.408	5.559	N/A
154	9.452	11.396	8.032	N/A
161	9.556	11.327	11.61	N/A
168	9.909	11.281	23.01	N/A
175	9.900	11.325	31.03	N/A
182	10.04	11.377	41.38	N/A
189	9.708	11.288	14.93	N/A
196	9.707	11.204	18.66	N/A
203	9.865	11.329	24.89	N/A
210	9.950	11.409	29.54	N/A

217	9.939	11.373	32.26	N/A
224	10.01	10.632	37.44	N/A
231	9.632	11.290	10.38	N/A
238	9.737	11.248	17.46	N/A
245	9.889	11.235	20.44	N/A
252	10.01	11.265	27.14	N/A
259	10.03	11.293	35.60	N/A
266	10.10	11.361	38.58	N/A

*not measured

Table 31. pH measurements of optimized 61V.

Sample	pH (Ci)	pH (Ce)
291	8.077	11.366
295	7.964	11.359
298	7.899	11.310
301	7.235	11.474
306	10.01	11.616
307	10.01	11.672
308	10.01	11.779
309	9.884	11.630
310	9.884	11.624
311	9.884	11.634
312	9.620	11.582
313	9.620	11.585
314	9.620	11.634
316	9.434	11.607
317	9.434	11.631
324	9.087	11.606

325	9.087	11.658
326	9.087	11.592
328	8.430	11.371
329	8.430	11.351
330	8.430	11.328
332	8.864	11.504
333	8.864	11.497
334	8.864	11.521
343	9.566	11.647
344	9.566	11.659
345	9.566	11.594
347	9.941	11.656
348	9.941	11.680
349	9.941	11.680
351	9.620	11.627
352	9.620	11.638
353	9.620	11.661
355	8.370	11.039
356	8.370	11.203
357	8.370	11.200
358	10.11	11.477

Table 32. Kinetics of original 61V.

			Ci	1	2	3	4	5	6
Sample	327	Time (h)	0.0000	0.9166	2.0666	2.9666	3.9333	5.3833	24.050
			00000	66667	66667	66667	33333	33333	00000
Date	7-apr	Concentration	575.17	520.87	518.83	517.52	500.68	499.86	496.67
		(mg/L)	36973	68177	42070	96753	99729	48123	40785

Slag weight (g)	0.2015	Qe (mg/g)	0.0000	5.3892	5.5920	5.7214	7.3929	7.4748	7.7915
			00000	68442	08963	91010	25491	27291	25440

Table 33. Kinetics of optimized 61V.

			Ci	1	2	3	4	5	6	7	8	9	10
Sample	315	Time (h)	0.00	0.93	2.08	2.96	3.95	5.40	6.30	8.21	24.0	25.2	26.7
			0000	3333	3333	6666	0000	0000	0000	6666	6666	8333	3333
			000	333	333	667	000	000	000	667	667	333	333
Date	7-apr	Concentration F (mg/L)	632.	544.	494.	464.	446.	432.	416.	398.	352.	334.	332.
			1944	8341	8626	5257	9534	7424	5269	2431	2798	3715	6435
			188	574	498	689	903	788	421	912	961	746	934
Slag weight (g)	0.1991	Qe (mg/g)	-	8.77	13.7	16.8	18.6	20.0	21.6	23.5	28.1	29.9	30.0
				5515	9525	4265	0782	3535	6423	0087	1798	1691	9048
				968	555	695	808	309	674	671	320	052	975